REPURPOSING THE *STREPTOCOCCUS MUTANS* CRISPR-CAS9 SYSTEM TO UNDERSTAND ESSENTIAL GENE FUNCTION

Shields RC[1], Walker AR[1], Maricic N[1], Underhill SAM[2], Burne RA[1]
[1]Department of Oral Biology, College of Dentistry, University of Florida, Gainesville, Florida, USA;
[2]Department of Physics, University of Florida, 2001 Museum Road, Gainesville, Florida, USA

ORCiDs:
Shields: http://orcid.org/0000-0002-8823-9504
Underhill: https://orcid.org/0000-0002-5214-4562
Burne: https://orcid.org/0000-0002-4234-0316

Keywords: Gene silencing, gene functional genomics, exopolysaccharides, cell division, dental caries

Corresponding Author Information:
Robert C. Shields
Department of Oral Biology
University of Florida College of Dentistry
1395 Center Drive
Gainesville, FL 32610
Phone: (352) 273-8850
Fax: (352) 273-8829
E-mail: rshields@dental.ufl.edu

Abstract

A recent genome-wide screen identified ~300 essential or growth-supporting genes in the dental caries pathogen *Streptococcus mutans*. To be able to study these genes, we built a CRISPR interference tool around the Cas9 nuclease ($Cas9_{Smu}$) encoded in the *S. mutans* UA159 genome. Using a xylose-inducible dead $Cas9_{Smu}$ with a constitutively active single-guide RNA (sgRNA), we observed titratable repression of GFP fluorescence that compared favorably to that of *Streptococcus pyogenes* dCas9 ($Cas9_{Spy}$). We then investigated sgRNA specificity and proto-spacer adjacent motif (PAM) requirements. Interference by sgRNAs did not occur with double or triple base-pair mutations, or if single base-pair mutations were in the 3' end of the sgRNA. Bioinformatic analysis of >450 *S. mutans* genomes allied with *in vivo* assays revealed a similar PAM recognition sequence as the $Cas9_{Spy}$. Next, we created a comprehensive library of sgRNA plasmids that were directed at essential and growth-supporting genes. We discovered growth defects for 77% of the CRISPRi strains expressing sgRNAs. Phenotypes of CRISPRi strains, across several biological pathways, were assessed using fluorescence microscopy. A variety of cell structure anomalies were observed, including segregational instability of the chromosome, enlarged cells, and ovococci-to-rod shape transitions. CRISPRi was also employed to observe how silencing of cell wall glycopolysaccharide biosynthesis (rhamnose-glucose polysaccharide, RGP) affected both cell division and pathogenesis in a wax worm model. The CRISPRi tool and sgRNA library are valuable resources for characterizing essential genes in *S. mutans*, some of which could prove to be promising therapeutic targets.

Introduction

Streptococcus species are natural inhabitants of humans and animals. Under the right conditions many streptococci can cause or exacerbate diverse infections in humans, including life-threatening illnesses that include meningitis or pneumonia [1]. The transition between commensalism and pathogenicity is an important feature of the oral streptococci, which is the most abundant bacterial genus in the human mouth [2]. Oral streptococci have important roles in the initiation and maturation of dental biofilms (plaque), and many are associated with oral and dental health. However, oral streptococci that are especially acidogenic and acid-tolerant are implicated as primary etiologic agents in the pathogenesis of dental caries (tooth decay) [3]. Dental caries is a common cause of pain, impaired quality of life, and tooth loss in children and adults [3]. The organism most often linked to caries development is *Streptococcus mutans*, which has been shown to have multiple virulence traits, some unique, that imbue the organism with the capacity to initiate and worsen the disease [4]. Extraorally, *S. mutans* and other oral streptococci can cause infective endocarditis [5]. More recently, epidemiologic and mechanistic studies point to a role for certain *S. mutans* strains in cardiovascular diseases, including stroke [6]. Investigating the biology of this organism is important for developing therapies that combat dental caries and other diseases associated with *S. mutans* and related organisms. More broadly, expanding the understanding of streptococcal biology will positively impact efforts to prevent or treat many other diseases in humans and animals.

Antimicrobial therapies usually target biological processes that are essential for bacterial growth and persistence. These pathways include protein synthesis, transcription, DNA replication, cell division, peptidoglycan biosynthesis, or folic acid metabolism. The most traditional approach for discovering new antibiotics has been screening the ability of natural and synthetic compounds to inhibit growth or processes essential for pathogenesis [7]. Alternatively, antibacterial targets could be identified by combining genome sequence data with genome-wide techniques that probe gene essentiality, followed by the identification or design of molecules that target the factors involved in the process of interest [8]. Global identification of essential genes is possible with a technique known as transposon sequencing (Tn-seq) [9]. Using Tn-seq, we identified a panel of genes that appears essential for the growth of *S. mutans* UA159, together with genes that are required for growth *in vitro* in rich or defined medium [10]. Although Tn-seq can be used to discover essential genes, it does not yield conditional mutations, and therefore does not allow for the functional study of these genes unless culture conditions can be found that allow for growth. Before moving toward studies that attempt to block or inhibit these pathways in *S. mutans*, or other streptococci, there is a need for further validation and investigation of these apparently essential genes. However, functional studies of essential genes in bacteria have traditionally been technically challenging and time-consuming, because mutants of these genes cannot be isolated and studied. One approach involves the generation of a conditional knockout, usually by mutating an essential gene and simultaneously expressing a copy of the gene under the control of a promoter that can be activated by an exogenously provided compound [11]. Two major drawbacks to this approach are that it is not easily adapted to a comprehensive study of the essential genome of an organism in a time-efficient manner (low throughput) and differences in gene expression levels between the conditional expresser and the wild type can generate misleading results.

Reprogramming of the bacterial CRISPR (clustered regularly interspaced short palindromic repeats) - Cas system into a gene-silencing tool has made it more practical to perform high-throughput studies of essential genes [12,13]. This technique, known as CRISPR interference (CRISPRi), combines an inducible, catalytically inactive *Streptococcus pyogenes* Cas9 nuclease, dead Cas9 (dCas9), with a programmable single-guide RNA (sgRNA). The sgRNA encodes a 20-nt sequence that is complementary to the target DNA. When expressed together in a cell, the sgRNA-dCas9$_{Spy}$ complex represses transcription initiation or elongation of the target gene. CRISPRi libraries that silence all putatively essential genes have been generated for both *Streptococcus pneumoniae* D39 [14] and *Bacillus subtilis* 168 [15]. A complicating factor for developing a CRISPRi system in *S. mutans* UA159 is

the presence of an endogenous Cas9 nuclease (SMu.1405c) [16]. Introduction of a CRISPRi system into *S. mutans* built around $dCas9_{Spy}$ would likely not function without the deletion of the endogenous Cas9, because of the potential for $Cas9_{Smu}$-sgRNA complexes to cause lethal double-strand breaks in the chromosome. In fact, $Cas9_{Smu}$ and $Cas9_{Spy}$ can cleave DNA in the presence of a *S. pyogenes* dual-RNA, and vice versa [17]. The Cas9 target recognition sequence, known as the proto-spacer adjacent motif (PAM), is also predicted to be 5'-NGG'-3' in *S. mutans*, as is the case in *S. pyogenes* [18]. Given the similarities, one possible approach to CRISPRi in *S. mutans* could be to repurpose the endogenous $Cas9_{Smu}$ nuclease into a nuclease-dead version, while also using elements of the original interference system (*e.g.* sgRNA). A CRISPRi system built around $Cas9_{Smu}$ could function more effectively in *S. mutans* than one based on $Cas9_{Spy}$. Heterologous expression of *S. pyogenes* dCas9 can be toxic to certain bacteria [19,20], although problems of this nature were not observed in a recent CRISPRi study in *S. pneumoniae* [14]. Irrespective of *S. pyogenes* dCas9 toxicity, the $dCas9_{Spy}$ could perform suboptimally compared to $dCas9_{Smu}$ simply due to codon-bias. Lastly, developing an *S. mutans* CRISPRi system has the potential to add to the number of tools for genome editing that are currently available.

Motivated by a desire to functionally study essential genes in *S. mutans,* we created a CRISPRi tool assembled around $dCas9_{Smu}$. We explored sgRNA specificity and PAM requirements, and compared interference activity with $dCas9_{Spy}$. Having demonstrated good CRISPRi activity, we then constructed a library of sgRNAs against all putative essential and growth-supporting genes [10]. With this library we evaluated growth and certain phenotypes in a subset of strains with CRISPRi-silenced essential genes. Finally, we used the technique to systematically study the impact that depletion of L-rhamnose-containing cell wall polysaccharides has on cell division and pathogenicity in an insect model.

Results

Robust gene knockdown with a titratable $dCas9_{Smu}$ system

More than 95% of the 477 *S. mutans* strains for which whole or draft genome sequences are presently available carry at least one CRISPR-Cas system (Fig 1A). The Type II-A CRISPR-Cas system, which can be repurposed for CRISPRi, is the most prevalent across the species with 339/477 strains carrying a complete system (Fig 1A). For reprogramming of *S. mutans* UA159 Cas9 (SMu.1405c) into a CRISPRi system, we began by mutating two amino acid residues (D10 and H840) known to be required for the nuclease activity of *S. pyogenes* Cas9 [21] (Fig 1B). We were able to confirm the DNA-binding and repressing activity of $dCas9_{Smu}$ by expressing a sgRNA against a constitutively expressed *gfp* gene [22] (Fig. 1C). Next, the *S. mutans dcas9* gene was cloned into pZX9 [23], such that expression could be activated by xylose. Prior to this, we discovered, using green fluorescent protein (GFP) as a readout for xylose-induced gene expression, that the P_{xyl} promoter was less active when glucose was the sole carbohydrate source compared to maltose (Fig S1). We suspect the different expression levels on glucose versus maltose could be due to carbohydrate catabolite repression and/or effects of certain phosphoenolpyruvate:sugar phosphotransferase system (PTS) components on P_{xyl} activity. Thus, we used the defined media 'FMC' containing maltose for all CRISPRi related experiments. To make the CRISPRi strain (Fig 1D), the sgRNA plasmid was integrated in single copy into the *S. mutans* genome in a strain that contained i) a *gfp* gene driven by the constitutively active P23 promoter and integrated into the chromosome, ii) the P_{xyl}-$dcas9_{Smu}$ plasmid and iii) point mutations that prevent translation of SMu.1405c (*cas9*; start codon mutated to stop codon). *S. mutans* Cas9 must be mutated, otherwise endogenous *cas9* expression in combination with sgRNAs would likely cause lethal chromosome damage; *S. mutans* is unable to repair the double-strand cleavage catalyzed by a functional Cas9.

Having developed the system, we moved to assessing its efficiency. Using the *S. mutans* CRISPRi technique, we observed titratable repression of GFP fluorescence (Fig 1E) and GFP protein levels (Fig 1F). Importantly, there were no obvious effects on the growth *S. mutans* as increasing amounts of xylose were added (up to 0.025% w/v). Also of note, slightly higher amounts of xylose (0.025% vs.

147 0.00625%) were required to achieve similar levels of repression of GFP production in a strain
148 containing a xylose-inducible *S. pyogenes dcas9* (Figs 1E and F). We also observed slight growth
149 impairments as increasing amounts of $dCas9_{Spy}$ were produced (Fig 1E). Overall, the differences in
150 performance of the two Cas9 constructs were minor. Lastly, we measured gene-silencing (absence of
151 GFP fluorescence) at the single-cell level (Fig S2). The number of cells escaping CRISPRi-mediated
152 gene knockdown (GFP positive) was very small, indicating that, at saturating amounts of xylose, the
153 effects of the *S. mutans*-derived CRISPRi system are uniform across the population when the dCas9
154 protein is delivered on a multi-copy plasmid.
155
156 **Guide RNA design principles for the sgRNA-$Cas9_{Smu}$ system**
157 To begin to optimize the *S. mutans* CRISPRi system, we examined parameters that are important for
158 functionality; the first of these was sgRNA specificity. sgRNA-Cas9 systems that operate with lower
159 sequence stringency could be prone to off-target effects that occur when guide RNA and dCas9 bind to
160 a site(s) in the genome that was not intended to be affected. To test this, we cloned an sgRNA with a
161 complementary sequence for the gene *atpB*, which encodes the beta subunit of the F_1F_O proton-
162 translocating ATPase. We modified the sgRNA-*atpB* sequence by introducing substitutions along the
163 length of guide RNA (Fig 2A). The sgRNA plasmids were added to competent *S. mutans* and plated
164 onto selective agar. We expected that transformation into *S. mutans* of the sgRNA-*atpB* plasmid lacking
165 sequence modifications would not be tolerated, leading to a very low transformation efficiency. As
166 expected, transformation of the sgRNA-$atpB^T$ (T; targeting the template strand) occurred at very low
167 efficiency, 1×10^{-5} (Fig 2B). Conversely, transformation efficiency in a Δ*cas9* (deletion of Smu.1405c)
168 strain, the dead *cas9* strain, or in a strain carrying a deletion of 20-bp of the $atpB^T$ sequence from the
169 sgRNA (sgRNAneg) was 100- to 1000-fold more efficient than with the intact *atpB* sgRNA (Fig 2B).
170
171 We next evaluated the effects of expressing sgRNAs with one, two or three base mutations within the
172 $atpB^T$ sequence. Single base-pair mismatches were tolerated at the 5' end of the sgRNA (*atpB*_3,
173 *atpB*_6, *atpB*_9 and *atpB*_12). Plasmids with mismatches closer to the PAM (*atpB*_15 and *atpB*_18)
174 transformed with higher efficiency into *S. mutans*, indicative of a loss of sgRNA activity. All of the
175 double and triple base mismatches reduced the activity of the sgRNAs, as these plasmids transformed
176 *S. mutans* at levels comparable to the *cas9*-deficient strain (Fig 2B). These results suggest that near
177 perfect sgRNA sequence complementarity is required to silence genes, and thus it should be possible
178 to minimize off-target effects with careful design of sgRNAs.
179
180 Another important feature of CRISPR-Cas9 systems, both as a natural bacterial immune system and
181 for CRISPRi, is the proto-spacer adjacent motif (PAM). This sequence is required for the Cas9 protein
182 to recognize interference targets and is also critical during the acquisition of CRISPR spacers (for Type
183 II-A systems) [21,24]. For a given bacterial strain, Type II-A PAM sequences are generated by aligning
184 CRISPR spacers to phage genomes, extracting the sequence downstream of the spacer target, and
185 then building a conserved sequence from these. The difficulty with taking this approach with *S. mutans*
186 UA159 is that there are too few CRISPR spacers from which to build a reliable PAM sequence.
187 Consequently, we compiled PAM sequences from a large (>450) collection of *S. mutans* genomes.
188 After narrowing the data to strains that had Type II-A CRISPR-Cas systems and ≥5 spacers, PAM
189 sequences were generated for 100 individual *S. mutans* strains using WebLogo (Fig S3). Per this
190 bioinformatics analysis, a highly conserved PAM for $Cas9_{Smu}$ was not evident. Rather, a significant
191 number of *S. mutans* strains with Cas9 contained spacers that might require the 5'-NGG-3' recognition
192 sequence for phage DNA interference, and these spacer arrays grouped together by alignment (Fig 3A,
193 yellow color). For other *S. mutans* strains with Cas9, PAM sequences were more random, but at least
194 two other groups, 5'-TTN-3' and 5'-NAAA-3', existed (Fig S3). We observed no obvious grouping for *S.*
195 *mutans* of the predicted PAM sequences by Cas9 protein identity (Fig 3A). We reasoned that PAM
196 recognition might be protein sequence specific and thus expected that the different PAM groups
197 predicted by bioinformatics would also group together. A lack of coherence between the predicted PAM

198 sequences and Cas9 protein sequences suggests that the PAM sequences assembled via
199 bioinformatics may not be the best indicator of the requirements for recognition for all *S. mutans* strains.
200 So, to investigate DNA recognition in greater detail we developed an interference assay with GFP
201 fluorescence as the readout. Using site-directed mutagenesis we incorporated assorted PAMs into a
202 construct in which the P23 promoter could drive the expression of a *gfp* gene (Fig 3B). This assay
203 confirmed that *S. mutans* dCas9 recognizes a 5'-NGG-3' PAM (Fig 3C). With 5'-NAG-3' we observed
204 moderate CRISPRi activity with $dCas9_{Smu}$, although the results varied as a function of the DNA base
205 present in the first position, with up to an 80% loss of GFP fluorescence. Weak binding of *S. pyogenes*
206 Cas9 to a 5'-NAG-3' PAM has been reported before [25–27]. Nuclease activity via 5'-NGA-3'
207 recognition has previously been reported for $Cas9_{Spy}$ [26,27] but we were unable to observe CRISPRi
208 activity with either dCas9 protein with a 5'-AGA-3' PAM. No interference was observed with any of the
209 other PAM sequence combinations tested.
210
211 **Creation of a comprehensive library of essential gene targeting sgRNAs**
212 We constructed a library of sgRNAs targeting 253 potentially essential and growth supporting genes
213 (Fig 4A). These genes (Table S1) were selected from previously conducted Tn-seq experiments [10],
214 Tn-seq performed as part of this study, and genes shown to be essential in previous studies (e.g.
215 *vicR/walR*). We were unable to design sgRNAs for 21 putative essential or growth supporting genes, of
216 which over half (12) were ribosomal proteins. These genes were small (average size of 275-bp) and
217 generally lacked PAM sites that would give desirable sgRNA sequences (*e.g.* RNA folding, off-target
218 effects, location in 5' region of gene). During the first round of cloning (see Materials and Methods) we
219 obtained correct sgRNA clones for 181 of 282 (64%) of the desired strains. After three rounds of
220 cloning 259/282 (92%) of the sgRNAs were successfully cloned. We were unable to obtain sgRNA
221 clones for 23 (8%) genes. After plasmid cloning in *E. coli* 10-beta, sequence-verified sgRNA plasmids
222 were transformed into *S. mutans* Δ*cas9* P_{xyl}-$dcas9_{Smu}$. While it would be possible to clone the sgRNA
223 plasmids directly into *S. mutans*, we wanted to minimize the number of passages in *S. mutans* as
224 CRISPRi strains are known to acquire suppressors when guide RNAs are expressed in their hosts [14].
225
226 **Growth phenotypes of strains with silenced essential genes**
227 We measured the growth of each sgRNA strain in FMC-maltose either in the absence or presence of
228 0.1% xylose for 16 h using a Bioscreen C Automated Microbiology Growth Curve System. Afterwards,
229 the area under the curve (AUC) was calculated for both conditions. Quantification of growth by AUC is
230 useful as it combines growth phases (lag, exponential and stationary phases). For each strain, the
231 AUC_{xylose} was divided by $AUC_{uninduced}$. Growth phenotypes were grouped per these ratios: >0.5, no
232 phenotype; 0.25-0.49, moderate growth defect; >0.25, strong growth defect). Growth defects were
233 observed in 194/253 (77%) of the strains expressing sgRNAs that were designed to target essential or
234 growth supporting genes (Fig 4B; S1 Table). Overall, we observed a higher percentage of growth
235 defects for strains with silenced essential genes versus growth-supporting genes, 82% and 62%,
236 respectively (Fig 4B). When comparing between different Clusters of Orthologous Groups (COGs), the
237 lowest median growth defects were observed for silenced genes in the translation (J) and lipid
238 metabolism and transport pathways (I) (Fig 4C). The highest median growth defects were observed
239 when sgRNAs targeted genes related to coenzyme transport and metabolism (H) and signal
240 transduction mechanisms (T) (Fig 4C). Growth defects were not observed for the six sgRNAs that
241 targeted non-essential genes. There was no significant relationship between the growth defect we
242 observed and the position of the sgRNA within the gene or the size of the target gene (Fig. S4).
243
244 **Assessing cell biology phenotypes of CRISPRi strains with microscopy**
245 Next we evaluated the morphological phenotypes of eighty CRISPRi strains placed in the following
246 functional categories: fatty acid biosynthesis/membrane biogenesis, peptidoglycan synthesis,
247 glycolysis, DNA replication, transcription, translation, cell division, and ATP synthase activity. Using
248 DAPI staining, we were able to visualize the bacterial chromosome, and with nile red we could detect

249 the cell membrane. The cell morphology defects of essential gene-targeted strains were diverse (Fig 5).
250 Defects included increased cell chaining, abnormally large cells, heterogeneously sized cells, cell lysis
251 and anucleate cells (Figs S5-S12). The most commonly observed morphological phenotypes across all
252 the pathways investigated were increased cell chaining (*e.g. pfk*, *accD*, *dnaE*, *rs3*, *atpC*) and
253 heterogeneously sized cells (*e.g. pgi*, *glmM*, *dnaG*, *eftS*, *atpF*) (Fig. 5A). It is important to note that
254 there were strains without obvious growth defects that displayed major cell morphology defects (*e.g.*
255 *ftsX* and *glmS*). Repression of genes involved in the glycolysis pathway led to significant growth defects
256 and larger/misshapen cells (Fig S5). When *pgm*, encoding phosphoglucomutase, was repressed, cells
257 appeared to be somewhat rod-shaped, probably associated with altered or deficient biosynthesis of cell
258 wall polysaccharides. When genes involved in peptidoglycan biosynthesis were repressed, the most
259 common phenotype was the formation of singular large round cells (Fig S6). The percentage of cells
260 displaying this phenotype varied, with it being most common in a strain with silenced *murM*, which in *S.*
261 *pneumoniae* encodes a protein that incorporates amino acids into the side-chain of peptidoglycan [28].
262 Repression of genes involved in the conversion of acetyl-CoA to malonyl-CoA (*accACD* and *bccP*), an
263 important step in fatty acid biosynthesis, led to excessive chaining of cells (Fig S7). Repression of fatty
264 acid biosynthetic (*fab*) genes yielded minor phenotypic changes, whereas silencing of genes
265 downstream of the FAS II pathway (*plsX* and *cdsA*) led to more obvious morphological defects. As
266 anticipated, when genes involved in DNA replication were repressed, not all cells contained nucleoids
267 (Fig S8). In addition to anucleate cells, certain CRISPRi strains with repressed chromosome replication
268 also showed severe morphological defects (e.g. *dnaE*, *dnaG*, *priA*). CRISPRi repression of translation-
269 related genes increased cell chaining (Fig S9). When the ribosomal proteins *rs3* (small ribosomal
270 subunit) and *rl11* (large ribosomal subunit) were repressed, we observed anucleate cells that lacked a
271 well-defined cell envelope. CRISPRi silencing of genes encoding subunits of the F_1F_O-ATPase led to
272 strong growth defects, increased cell chaining and variability in nile red staining (Fig S10). Repression
273 of transcription-related genes also led to increased cell chaining and attenuated growth (Fig S11). The
274 cell shape and size of *rpoB*-, *rpoC*-, and *rpoZ*-silenced CRISPRi strains were severely impacted. When
275 genes involved in cell division were repressed, strains displayed heterogeneity in cell size and shape
276 (Fig S12). Notably, with repression of *divIC*, *ftsA*, *ftsL* and *ftsZ* we observed similar morphological
277 changes. Cells appeared to be rod-shaped, except that they bulged at the cell septum, probably
278 consistent with an inability of these cells to complete septation. FtsZ is a tubulin homologue that forms
279 a Z-ring at the midcell that is important for scaffolding and cytokinesis [29]. FtsA, DivIC and FtsL also
280 localize to the midcell (at different stages) during cell division [29]. Repression of *gbpB* (glucan-binding
281 protein B), an ortholog of the *S. pneumoniae* peptidoglycan hydrolase gene, *pcsB*, led to cell division
282 defects. Although specific peptidoglycan hydrolase activity has not been observed for GbpB, the cell
283 division defects we observed, along with the observation that GbpB can be localized to areas of active
284 peptidoglycan synthesis [30], provide support for the idea that it may act enzymatically to affect the
285 structure of the cell wall. Taken together, microscopic analysis of CRISPRi strains from different
286 pathways has revealed generalized phenotypes of essential gene depletion, but also clear functional
287 links between genes in established pathways.
288
289 **L-rhamnose glycopolymers are critical for *S. mutans* cell division and pathogenicity**
290 Having shown that CRISPRi allows for the functional study of essential genes, we next focused our
291 attention on a pathway that is thought to be of major importance to *S. mutans*, rhamnose-glucose
292 polysaccharide (RGP) biosynthesis. Certain streptococcal species lack cell wall teichoic acids (WTAs)
293 and instead produce RGPs that are covalently linked to the peptidoglycan [31]. RGP biosynthesis
294 begins with a four-step pathway encoded by the genes *rmlABCD* that converts glucose-1-phosphate
295 into dTDP-L-rhamnose. The last gene in the pathway, *rmlD*, resides in an operon (SMu.824-835) that
296 contains genes required for additional RGP biosynthesis steps and transport of the carbohydrates
297 through the cell membrane. By our Tn-seq analysis, most of the genes involved in producing RGP are
298 either essential or required for the growth of *S. mutans* UA159 (Fig 6A) [10]. L-rhamnose biosynthetic
299 pathways are also essential in *S. pyogenes* [32] and *Mycobacterium smegmatis* [33]. Several of these

genes have, however, been mutated in *S. mutans*, including *rmlBC* [34], *rmlD* [32], *rgpE* [30,35], *rgpF* [35,36], and *rgpG* [37]. Inconsistencies between our observations and others could be related to the nature of our Tn-seq selection and/or the presence of undetected suppressor mutations that bypass essentiality in strains that carry RGP gene deletions in other studies. Use of CRISPRi to study RGP function facilitates the rapid evaluation of depleting each gene product under conditions that allow for selective pressure to be applied only when xylose is provided in the medium. By CRISPRi, down-regulation of every gene directly involved in RGP biosynthesis displayed severe growth defects when silenced with sgRNAs (Fig 6B; Fig S13). In the invertebrate infection model organism *Galleria mellonella*, strains with silenced *rmlB*, *rgpC*, and *rgpF* genes displayed attenuated virulence compared to wild-type *S. mutans* UA159 and a d*cas9* strain (Fig 6C). For this proof-of-concept study, sgRNAs were expressed in an *S. mutans* strain where the endogenous Cas9 had been converted to dCas9. A strain with silenced *rmlD* was not attenuated. However, we suspect this strain acquired suppressor mutation(s) as it originally grew very poorly, but after some passage it was able to grow to a final OD_{600} similar to the parental strain. Having shown that RGP biosynthesis genes are required for growth in laboratory media and during infection, we next investigated their importance to *S. mutans* cell biology. Consistent with previous observations [30,37], cellular morphologies were exceptionally aberrant, compared to the wild type (Fig S13). Cells were large, not consistently ovococcoid, and formed longer chains than normal. Although resolutions were limiting, it also appeared that certain large cells contained multiple nucleoids by DAPI strain (Fig S14). To gain greater ultrastructural insights, we investigated cell biology phenotypes of *rmlB*, *rmlD*, *rgpC*, and *rgpF* silenced strains with transmission electron microscopy (TEM). In these strains, division site positioning was irregular and not always in the mid-point of cells (Fig 6D). There were instances where the division septum was unable to traverse the cell (*rmlB*, *rmlD, rgpF*) or cells had double septa (*rgpF*) (Fig 6D). Accordingly, large cells with incomplete septation appeared to have multiple unequally sized compartments, which likely has a deleterious effect on chromosome segregation, and might explain the unusual patterns of DAPI staining observed during fluorescence microscopy. In *rgpC*-silenced cells, the equatorial ring, an outgrowth of cell wall material that is normally duplicated and separates as cells divide, was abnormally thick and in some cases was 'peeling' back from the cell (Fig 6D). Measurements from the CRISPRi strain micrographs using ImageJ confirmed that they were wider than wild-type cells (Fig 6E).

Discussion

Essential genes represent promising targets for antimicrobials. The essential genome of *S. mutans* is comprised of ~300 genes and, like other bacteria, is enriched for genes that function in processing genetic information, energy production, and maintenance of the cell envelope. However, until the recent development of CRISPRi technologies, high-throughput functional studies of these genes has not been possible. Here we demonstrate the conversion of the *S. mutans* Cas9 nuclease into a gene silencing tool for the systematic interrogation of the essential genome. Our system is relatively streamlined as it only requires a constitutively expressed sgRNA and a xylose-inducible dCas9. Importantly, it allowed us to study all the known essential genes in a relatively short time. Most of the genes predicted to be essential by Tn-seq displayed strong growth defects once silenced by CRISPRi. Furthermore, CRISPRi strains with sgRNAs targeting essential genes displayed morphological defects when analyzed by microscopy. This work confirms the importance of these genes to the integrity of *S. mutans* cells, and of their potential as interesting therapeutic targets for the control of *S. mutans* or certain other pathogenic streptococci.

One interesting finding of this work is that $Cas9_{Smu}$ recognition of target DNA shares similarities with $Cas9_{Spy}$. First, guide RNA specificity of $Cas9_{Smu}$ is similar to $Cas9_{Spy}$ as single base-pair mismatches are not tolerated in the 5' region of sgRNA (the seed region) [38,39]. $Cas9_{Smu}$ was also unable to cause DNA cleavage *in vivo* when double or triple base-pair mutations were introduced into the sgRNA sequence, again consistent with findings in $Cas9_{Spy}$ [39]. Second, PAM recognition relied on a 5'-NGG-3' sequence. We also observed moderate CRISPRi activity with a 5'-NAG-3' PAM. $Cas9_{Spy}$ activity also

351 relies on a 5'-NGG-3' PAM with weak DNA recognition reported for the non-canonical PAMs 5'-NAG-3'
352 and 5'-NGA-3' [25–27], although we were unable to measure this with our assay. Although target
353 recognition also relies on other factors [40], we are confident that off-target effects should be minimized
354 when using a 5'-NGG-3' PAM and a guide RNA designed to ensure a lack of complementarity (two or
355 more mismatches) to other regions of the genome. The similarities of $Cas9_{Smu}$ and $Cas9_{Spy}$ are
356 interesting given that other streptococcal Cas9 nucleases require PAMs that differ to 5'-NGG-3' [20,41].
357 For example, the Cas9 of *Streptococcus canis*, which shares ~90% sequence similarity to $Cas9_{Spy}$,
358 recognizes a 5'-NNG-3' PAM [41]. Bioinformatics analysis of the species-wide PAM requirements were
359 cryptic, but it is possible that other *S. mutans* Cas9 proteins recognize alternative PAMs *e.g.* 5'-NAAA-
360 3'. Intriguingly the Cas9 of *Streptococcus macacae* NCTC 11558 is presumed to recognize an adenine
361 enriched PAM [42]. There is an arms race between the bacteria that generate Cas9 proteins
362 recognizing new PAMs and the phage that undergo mutations to avoid CRISPR interference, with the
363 latter being a confounding issue with PAMs that are generated solely using bioinformatic tools. Despite
364 these limitations, it is possible there is species-wide PAM diversity, similar to what has been observed
365 with *Neisseria meningitidis* [43]. This is an interesting area of study as it should aid in the engineering of
366 new variants of Cas9 that recognize different PAMs, thus expanding the genetic engineering
367 capabilities of the Cas9 proteins.
368
369 The CRISPRi system described here was able to perturb the expression of over 250 putative essential
370 and growth-supporting genes. The severe growth defects exhibited by most of these strains
371 emphasizes their critical functions in *S. mutans*. The percentage of silenced genes that displayed
372 significant growth defects was comparable with what was observed for *S. pneumoniae* [14]. As noted
373 above, CRISPRi has many advantages over more traditional approaches for studying essential genes,
374 but the technique has its limitations. For example, failure to display an aberrant growth phenotype could
375 be caused by sub-optimal sgRNA design or selection for suppressor mutations that bypass essentiality.
376 Likewise, certain essential genes could still function with a low number of protein molecules per cell if
377 the target gene is no completely silenced. In some cases, strains that displayed relatively minor growth
378 defects when the target genes were depleted had significant alterations in cell morphology. Tn-seq,
379 which was used to identify to candidate genes for this study (REF), is a competitive assay, so even
380 mutants with minor growth phenotypes could be significantly underrepresented at the chosen end-point.
381 In this study, we supplemented our previous Tn-seq essential gene analysis [10] with a different Tn-seq
382 approach, which involved plating the original library on BHI instead of blood agar, then passaging the
383 libraries in BHI or FMC for ~10 generations, as compared with ~30 generations in our previous study
384 (REF). The differences between the older and the newer Tn-seq analysis were minor (Table S1).
385 Overall, the CRISPRi growth study paired with comprehensive Tn-seq enquiries provide a solid
386 foundation for determining which genes are essential in *S. mutans* UA159. It is reasonable to predict
387 that some of these gene products could be targeted for the therapeutic control of *S. mutans* and
388 possibly some other pathogenic streptococci.
389
390 In addition to growth studies, we were able to observe morphological phenotypes of CRISPRi strains
391 with light and electron microscopy. Several morphology phenotypes were evident that were consistent
392 with other high-throughput microscopic studies of essential gene depletions [14,15]. The changes in
393 morphology could represent more generalized responses to an inability to grow or, in some cases, may
394 prove useful in linking gene products that function in concert. For example, *ftsA*, *ftsZ*, *ftsL* and *divIC*
395 shared similar phenotypes, consistent with their products being required for correct cell septum
396 formation. Perturbation of peptidoglycan synthesis led in some cases to the formation of large round
397 cells. Blocking or deleting peptidoglycan synthesis genes in other bacteria can lead to the generation of
398 giant cells [44] or L-forms [45], although the phenotypes in this study appear distinct from those
399 previously described variants.
400

401 The rhamnose-glucose polysaccharide (RGP) of mutans streptococci were used in the past to
402 differentiate serotypes of strains that were previously all designated as *S. mutans.* Today, it is
403 recognized that the species *S. mutans* consists primarily of Bratthall serotypes *c, e,* and *f*, along with
404 the unusual serotype *k* strains [46,47]. In contrast, what was formerly designated serotype *b S. mutans*
405 is now classified as *Streptococcus ratti*. It is also now well recognized that RGP is an important
406 constituent of the envelope of mutans streptococci. Clear impacts on growth, pathogenicity and cell
407 division were observed in strains that had silenced genes contributing to RGP biogenesis. The cell
408 morphology phenotypes were stark, with depletion strains clearly exhibiting aberrant septum formation,
409 as has been noted before in *S. mutans* and other related species [30,48,49]. An inability to divide
410 normally has been linked to aberrant localization of the peptidoglycan hydrolase PcsB (GbpB in *S.*
411 *mutans*) [30,49]. When *gbpB* was targeted with CRISPRi, cells appeared to be unable to divide
412 correctly (Fig S12), but the phenotype did not match that associated with *rgp* gene silencing. Given the
413 vital role and essentiality of the RGP biosynthetic pathway, coupled with the decreased virulence of
414 certain *rgp* knockdowns reported here, RGP biogenesis may be an attractive antimicrobial target.
415 Further, if RGP and peptidoglycan synthesis are linked, it is conceivable that targeting RGP
416 biosynthesis could potentiate the efficacy of β-lactam and other cell wall-active antibiotics. Other
417 attractive aspects of the RGP pathway as an antimicrobial target include the species or strain-specificity
418 of the glycopolymers and the absence of the pathway in humans [31].
419
420 In summary, this is the first study to utilize CRISPRi in *S. mutans* as a genetic tool. We did so by
421 repurposing the Cas9 that is widely distributed among the species, opening new avenues for
422 investigating the diversity of CRISPR-Cas in *S. mutans* and other oral streptococci, and the possible
423 development of next-generation CRISPR-Cas tools. We demonstrate that the technique provides a
424 powerful approach for studying essential genes and gene function, in agreement with studies using
425 other organisms [14,15]. We anticipate that these tools can be used to investigate new aspects of *S.*
426 *mutans* cell biology and to identify promising therapeutic candidates.
427
428 **Materials and methods**
429 **Bacterial strains and growth conditions.** Strains of *Streptococcus mutans* were cultured in Brain
430 Heart Infusion (BHI) broth (Difco) or chemically defined medium (FMC) [50] supplemented with 0.5%
431 maltose. Streptococci were grown in a 5% CO_2 aerobic environment at 37°C, unless stated otherwise.
432 Strains of *Escherichia coli* were routinely grown in lysogeny broth (LB) with slight modifications (Lennox
433 LB; 10 g/L tryptone, 5 g/L yeast extract and 5 g/L NaCl) at 37°C with aeration. Antibiotics were added to
434 growth media at the following concentrations: kanamycin (1.0 mg/ml for *S. mutans*, 50 µg/ml for *E. coli*),
435 erythromycin (10 µg/ml for *S. mutans*, 300 µg/ml for *E. coli*), spectinomycin (1.0 mg/ml for *S. mutans*,
436 50 µg/ml for *E. coli*) and ampicillin (100 µg/ml for *E. coli*). Strains and plasmids are listed in S2 Table.
437
438 **CRISPR-Cas bioinformatics.** The 477 *S. mutans* genomes available in the National Center for
439 Biotechnology Information (NCBI) GenBank in June 2018 were mined using CRISPRone [51] to
440 determine the occurrence and diversity of CRISPR-Cas systems in this species. CRISPR arrays were
441 also identified using CRISPRone and these were used to predict the PAM sequence based on spacer-
442 protospacer matches using CRISPRTarget [52]. Afterwards, consensus PAM sequences for each strain
443 were built using the WebLogo server [53].
444
445 **Construction of the xylose-inducible CRISPRi system.** Xylose-inducible plasmids were cloned by
446 following a protocol developed by Xie *et al* [23]. Three plasmids were generated that contained *gfp*,
447 $dcas9_{Smu}$ and $dcas9_{Spy}$ inserts cloned into the pZX9 plasmid. For each plasmid, two linear fragments
448 were created by PCR using pZX9 or *S. mutans* UA159 genomic DNA as templates. $dcas9_{Spy}$ was
449 amplified from a plasmid obtained from Addgene (Addgene #44249). $dcas9_{Smu}$ was amplified from the
450 strain described in the supplemental material. The *gfp* gene was amplified from previously constructed
451 *gfp*-reporter strains [22]. The PCR fragments are designed so that they have overlapping

452 complementary regions that facilitate concatemer formation during a 2nd PCR. The products generated
453 by this 2nd PCR are transformed directly into *S. mutans*. Primers pZX9seqF and pZX9seqR were used
454 to amplify gene inserts followed by Sanger sequencing. For cloning of the sgRNA plasmid
455 (pPM::sgRNA), a synthetic DNA fragment was generated (Integrated DNA Technologies) that
456 contained the following components sequentially: 1) a P_{veg} promoter [22], 2) a 20-nt sgRNA targeting
457 *gfp*, 3) a 42-nt dCas9 binding handle sequence, and 4) an *S. pyogenes* terminator. Restriction enzyme
458 recognition sequences for *Sac*I and *Sph*I were included at the 5' and 3' ends of the sgRNA construct
459 respectively. The synthetic DNA fragment was subsequently cloned into the pPMZ plasmid which
460 integrates at the *phnA-mtlA* locus of *S. mutans* UA159. This plasmid was also used to generate
461 plasmids containing sgRNAs that target other areas of the *S. mutans* genome. Protocols for cloning of
462 additional strains are provided in S1 File. Oligonucleotides used in this study are listed in S3 Table.
463
464 **Green fluorescent protein CRISPRi assay.** To test the CRISPRi system and compare the activity of
465 $dCas9_{Smu}$ to $dCas9_{Spy}$ we used a GFP based assay. CRISPRi strains were cultured overnight, grown to
466 an OD_{600} = 0.5, and then diluted 1:100 into FMC-maltose with or without xylose. For these assays the
467 concentration of xylose was serially diluted. In triplicates, 200 µL samples were added to clear-
468 bottomed, black-sided, 96-well microtiter plates. After loading of the cultures, the 96-well plate was
469 placed in a Synergy HT microtiter plate reader (BioTek). The fluorescence and optical density
470 (absorbance at 600 nm) were measured at 30-min intervals using Gen5 software (BioTek). The
471 fluorescence settings were excitation at 485 nm, emission at 525 nm, and a sensitivity of 65. Data
472 readings were collected, and the background fluorescence or OD600 was subtracted prior to data
473 visualization using GraphPad Prism (v7) software (GraphPad Software). A slightly modified version of
474 this assay was used for PAM comparisons (S1 File). The protocol for Western blotting of GFP and
475 $dCas9_{Spy}$ is available in S1 File.
476
477 **sgRNA library design and cloning.** sgRNA sequences (20-nt) were selected with CRISPy-web [54].
478 With this tool we uploaded the *S. mutans* UA159 GenBank file (NC_004350.2) and selected essential
479 genes. For each gene, the tool designs sgRNAs with predicted off-target matches (13-bp upstream of
480 the PAM; off-targets containing 0, 1, 2, or 3-bp mismatches). To minimize off-target effects we only
481 selected sgRNAs with two or more mismatches, which we have shown to diminish sgRNA activity (Fig
482 2B). We also aimed to select sgRNA sequences as close to the start of each gene as possible. For
483 each sgRNA we predicted the secondary structure (20-nt sequence and 42-nt dCas9 binding handle)
484 with the RNAfold program provided by ViennaRNA [55]. Only sgRNAs that maintained the hairpin
485 structure of the dCas9 binding handle were selected for cloning. sgRNA sequences were cloned using
486 the Q5® Site-Directed Mutagenesis Kit (New England Biolabs). Primers were designed using the
487 NEBaseChanger™ tool (v.1.2.9), substituting the sgRNA-*gfp* 20-nt sequence for whichever sgRNA we
488 were cloning. Using the designed primers, the pPM::sgRNA plasmid was amplified and then added to a
489 mix of Kinase-Ligase-*Dpn*I for 5 min at room temperature. This mixture (5 µL) was then transformed
490 into chemically competent *E. coli* 10-beta with selection on LB-kanamycin. For each sgRNA plasmid
491 transformation, two independent clones were selected and cultured overnight. With each culture we
492 made a glycerol stock for storage at -80°C, and purified plasmid with the QIAprep Spin Miniprep Kit
493 (Qiagen). Each plasmid was Sanger sequenced using the pRCS1seqR primer (S3 Table).
494
495 **sgRNA plasmid interference assays.** sgRNA sequence specificity was tested using a plasmid
496 interference assay. A 20-nt sequence complementary to the template strand of the *atpB* gene
497 (SMu.1528) was introduced into the pPM::sgRNA plasmid with the Q5® Site-Directed Mutagenesis Kit.
498 Using the same kit, single, double, or triple base-pair mismatches were introduced into the 20-nt *atpB*
499 sgRNA sequence. These plasmids were transformed into competent *S. mutans* and cells were serially
500 diluted onto BHI agar, or BHI agar containing kanamycin. The percentage of cells that were
501 transformed was calculated from the colony forming units present on both types of agar.
502

503 **CRISPRi growth assays.** Strains of *S. mutans* carrying sgRNA cassettes were grown overnight in BHI
504 with the appropriate antibiotics in a microaerophilic environment at 37°C. The following day the
505 bacterial cultures were washed once in FMC-maltose, and then diluted 1:1000 into FMC-maltose or
506 FMC-maltose containing 0.025% xylose. Triplicates of 300 µL were added to a Bioscreen C 10 x 10
507 well plate for each condition. OD_{600} was measured every 30 min for 16 h with a Bioscreen C Automated
508 Microbiology Growth Curve Analysis System (Growth Curves USA).
509
510 **Fluorescence microscopy of CRISPRi strains.** Overnight cultures of CRISPRi strains were diluted
511 1:100 into 200 µL FMC-maltose containing 0.025% xylose, and then incubated at 37°C in a 5% CO_2
512 incubator for 16 h. After incubation, 1 µL of 1 mg/mL nile red (ThermoFisher Scientific) was added to
513 each sample and incubated for 5 min at room temperature (RT) in darkness. Next, 1 µL of 1 mg/mL
514 DAPI (4′,6-diamidino-2-phenylindole; ThermoFisher Scientific) was added to each sample and
515 incubated at RT in darkness for a further 5 min. Samples were centrifuged for 5 min at 4,000 x *g* and
516 suspended in ProLong™ Live Antifade Reagent (ThermoFisher Scientific). For imaging, 2.5 µL of
517 stained cells were placed on PBS (pH 7.4; 137 mM NaCl, 2.7 mM KCl, 8 mM Na_2HPO_4, 2 mM KH_2PO_4)
518 agarose pads [56] before sealing with a coverslip. Images were captured with a Zeiss Axiovert 200M
519 microscope equipped with a Zeiss AxioCam MRm camera using a 100X oil objective.
520
521 **Transmission electron microscopy.** CRISPRi strains were grown as described for fluorescence
522 microscopy. Afterwards cells were rinsed with 0.1M sodium cacodylate buffer and then fixed in 3%
523 glutaraldehyde overnight at 4˚C. The following day, cells were treated with 1.5% osmium tetroxide in
524 the dark for 1 h at 4˚C. Next the cells were mixed in equal parts with 5% agarose in PBS, collected by
525 centrifugation at 2000 x *g*, and cooled to 4°C. Small chunks of the bacterial pellet plus agarose were
526 then dehydrated in ethanol via the following steps: 30%, 50%, 70%, 80%, 90% each for 15 min, 99% 10
527 min, and then absolute ethanol 2 x 10 min. The dehydrated cells were embedded in an epoxy resin,
528 sectioned and stained with uranyl acetate and lead citrate. Microscopy was conducted using a Hitachi
529 H7600 transmission electron microscope.
530
531 **Waxworm experiments.** *Galleria mellonella* killing assays were performed as described previously
532 [57]. Insects in the final instar larval stage were purchased from Vanderhorst, Inc. (St. Marys, OH),
533 stored at 4°C in the dark and used within 7 days of shipment. Groups of 15 larvae, ranging in weight
534 from 200 to 300 mg and with no signs of melanization, were selected at random for subsequent
535 infection. Insects were injected with $1x10^7$ CFU of bacterial inoculum, prepared from overnight cultures
536 that had been washed and resuspended in 0.9% saline solution, into the hemocoel of each larva via the
537 last left proleg using a 25-µl Hamilton syringe. Fifteen larvae were injected for each condition. The
538 number of viable cells injected into the larvae was verified by colony counts on BHI plates. As a
539 negative control, one group of *G. mellonella* were injected with UA159 that was heat killed at 80°C for
540 30 minutes. After injection, insects were kept at 37°C and survival at different time intervals was
541 recorded. Larvae were scored as dead when thigmotaxis was absent. Kaplan-Meier killing curves were
542 plotted, and estimations of differences in survival were compared using a log rank test. All data were
543 analyzed with GraphPad Prism, version 7.0c software. Experiments were repeated three times.
544
545 **Data availability.** The datasets generated and analyzed during the current study are available from the
546 corresponding author on reasonable request.
547
548 **Acknowledgements**
549
550 We thank Dr. Sharon Matthews and Chao Chen at the Electron Microscopy core at the University of
551 Florida for help with TEM imaging and analysis; Dr. Vincent Richards for sending us the *S. mutans*
552 genomes; Dr. Justin Merritt for providing us with the pZX plasmids for xylose-inducible gene expression
553 in *S. mutans*; and Dr. Edward Chan and John Calise for use of, and technical assistance with,

fluorescence microscopy. This work was supported by National Institutes of Health grant R01DE013239 (to R.A.B.).

References

1. Krzyściak W, Pluskwa KK, Jurczak A, Kościelniak D. The pathogenicity of the Streptococcus genus. Eur J Clin Microbiol Infect Dis. 2013;32: 1361–1376. doi:10.1007/s10096-013-1914-9

2. Dewhirst FE, Chen T, Izard J, Paster BJ, Tanner ACR, Yu W-H, et al. The human oral microbiome. J Bacteriol. 2010;192: 5002–17. doi:10.1128/JB.00542-10

3. Pitts NB, Zero DT, Marsh PD, Ekstrand K, Weintraub JA, Ramos-Gomez F, et al. Dental caries. Nat Rev Dis Primer. 2017;3: 17030. doi:10.1038/nrdp.2017.30

4. Lemos JA, Quivey RG, Koo H, Abranches J. *Streptococcus mutans*: a new Gram-positive paradigm? Microbiology. 2013;159: 436–45. doi:10.1099/mic.0.066134-0

5. Nomura R, Nakano K, Nemoto H, Fujita K, Inagaki S, Takahashi T, et al. Isolation and characterization of *Streptococcus mutans* in heart valve and dental plaque specimens from a patient with infective endocarditis. J Med Microbiol. 2006;55: 1135–1140. doi:10.1099/jmm.0.46609-0

6. Nakano K, Hokamura K, Taniguchi N, Wada K, Kudo C, Nomura R, et al. The collagen-binding protein of *Streptococcus mutans*is involved in haemorrhagic stroke. Nat Commun. 2011;2: 485. doi:10.1038/ncomms1491

7. Lewis K. Platforms for antibiotic discovery. Nat Rev Drug Discov. 2013;12: 371–387. doi:10.1038/nrd3975

8. Juhas M, Eberl L, Church GM. Essential genes as antimicrobial targets and cornerstones of synthetic biology. Trends Biotechnol. 2012;30: 601–607. doi:10.1016/j.tibtech.2012.08.002

9. van Opijnen T, Bodi KL, Camilli A. Tn-seq: high-throughput parallel sequencing for fitness and genetic interaction studies in microorganisms. Nat Methods. 2009;6: 767–72. doi:10.1038/nmeth.1377

10. Shields RC, Zeng L, Culp DJ, Burne RA. Genomewide Identification of Essential Genes and Fitness Determinants of *Streptococcus mutans* UA159. mSphere. 2018;3: e00031-18. doi:10.1128/mSphere.00031-18

11. Fan F, Lunsford RD, Sylvester D, Fan J, Celesnik H, Iordanescu S, et al. Regulated Ectopic Expression and Allelic-Replacement Mutagenesis as a Method for Gene Essentiality Testing in *Staphylococcus aureus*. Plasmid. 2001;46: 71–75. doi:10.1006/plas.2001.1526

12. Bikard D, Jiang W, Samai P, Hochschild A, Zhang F, Marraffini LA. Programmable repression and activation of bacterial gene expression using an engineered CRISPR-Cas system. Nucleic Acids Res. 2013;41: 7429–7437. doi:10.1093/nar/gkt520

13. Qi LS, Larson MH, Gilbert LA, Doudna JA, Weissman JS, Arkin AP, et al. Repurposing CRISPR as an RNA-Guided Platform for Sequence-Specific Control of Gene Expression. Cell. 2013;152: 1173–1183. doi:10.1016/j.cell.2013.02.022

590 14. Liu X, Gallay C, Kjos M, Domenech A, Slager J, van Kessel SP, et al. High-throughput CRISPRi phenotyping
591 identifies new essential genes in *Streptococcus pneumoniae*. Mol Syst Biol. 2017;13: 931–931.
592 doi:10.15252/MSB.20167449

593 15. Peters JM, Colavin A, Shi H, Czarny TL, Larson MH, Wong S, et al. A Comprehensive, CRISPR-based Functional
594 Analysis of Essential Genes in Bacteria. Cell. 2016;165: 1493–1506. doi:10.1016/j.cell.2016.05.003

595 16. Serbanescu MA, Cordova M, Krastel K, Flick R, Beloglazova N, Latos A, et al. Role of the *Streptococcus*
596 *mutans* CRISPR-Cas Systems in Immunity and Cell Physiology. J Bacteriol. 2015;197: 749–761.
597 doi:10.1128/JB.02333-14

598 17. Fonfara I, Le Rhun A, Chylinski K, Makarova KS, Lécrivain A-L, Bzdrenga J, et al. Phylogeny of Cas9
599 determines functional exchangeability of dual-RNA and Cas9 among orthologous type II CRISPR-Cas
600 systems. Nucleic Acids Res. 2014;42: 2577–2590. doi:10.1093/nar/gkt1074

601 18. van der Ploeg JR. Analysis of CRISPR in *Streptococcus mutans* suggests frequent occurrence of acquired
602 immunity against infection by M102-like bacteriophages. Microbiol Read Engl. 2009;155: 1966–1976.
603 doi:10.1099/mic.0.027508-0

604 19. Cho S, Choe D, Lee E, Kim SC, Palsson B, Cho B-K. High-Level dCas9 Expression Induces Abnormal Cell
605 Morphology in *Escherichia coli*. ACS Synth Biol. 2018;7: 1085–1094. doi:10.1021/acssynbio.7b00462

606 20. Rock JM, Hopkins FF, Chavez A, Diallo M, Chase MR, Gerrick ER, et al. Programmable transcriptional
607 repression in mycobacteria using an orthogonal CRISPR interference platform. Nat Microbiol. 2017;2:
608 16274. doi:10.1038/nmicrobiol.2016.274

609 21. Jinek M, Chylinski K, Fonfara I, Hauer M, Doudna JA, Charpentier E. A Programmable Dual-RNA-Guided DNA
610 Endonuclease in Adaptive Bacterial Immunity. Science. 2012;337: 816–821. doi:10.1126/science.1225829

611 22. Shields RC, Kaspar JR, Lee K, Underhill S a. M, Burne RA. Fluorescence tools adapted for real-time monitoring
612 of the behaviors of *Streptococcus* species. Appl Environ Microbiol. 2019. doi:10.1128/AEM.00620-19

613 23. Xie Z, Qi F, Merritt J. Development of a tunable wide-range gene induction system useful for the study of
614 streptococcal toxin-antitoxin systems. Appl Environ Microbiol. 2013;79: 6375–84. doi:10.1128/AEM.02320-
615 13

616 24. Heler R, Samai P, Modell JW, Weiner C, Goldberg GW, Bikard D, et al. Cas9 specifies functional viral targets
617 during CRISPR–Cas adaptation. Nature. 2015;519: 199–202. doi:10.1038/nature14245

618 25. Leenay RT, Maksimchuk KR, Slotkowski RA, Agrawal RN, Gomaa AA, Briner AE, et al. Identifying and
619 Visualizing Functional PAM Diversity across CRISPR-Cas Systems. Mol Cell. 2016;62: 137–147.
620 doi:10.1016/j.molcel.2016.02.031

621 26. Zhang Y, Ge X, Yang F, Zhang L, Zheng J, Tan X, et al. Comparison of non-canonical PAMs for CRISPR/Cas9-
622 mediated DNA cleavage in human cells. Sci Rep. 2014;4. doi:10.1038/srep05405

623 27. Kleinstiver BP, Prew MS, Tsai SQ, Topkar V, Nguyen NT, Zheng Z, et al. Engineered CRISPR-Cas9 nucleases
624 with altered PAM specificities. Nature. 2015;523: 481–485. doi:10.1038/nature14592

625 28. Filipe SR, Tomasz A. Inhibition of the expression of penicillin resistance in *Streptococcus pneumoniae* by
626 inactivation of cell wall muropeptide branching genes. Proc Natl Acad Sci U S A. 2000;97: 4891–4896.
627 doi:10.1073/pnas.080067697

628 29. Massidda O, Nováková L, Vollmer W. From models to pathogens: how much have we learned about
629 *Streptococcus pneumoniae* cell division? Environ Microbiol. 2013;15: 3133–3157. doi:10.1111/1462-
630 2920.12189

631 30. Kovacs CJ, Faustoferri RC, Bischer AP, Quivey RG. *Streptococcus mutans* requires mature rhamnose-glucose
632 polysaccharides for proper pathophysiology, morphogenesis and cellular division. In: Molecular
633 Microbiology [Internet]. 12 Jul 2019 [cited 14 Aug 2019]. doi:10.1111/mmi.14330

634 31. Mistou M-Y, Sutcliffe IC, van Sorge NM. Bacterial glycobiology: rhamnose-containing cell wall
635 polysaccharides in Gram-positive bacteria. FEMS Microbiol Rev. 2016;40: 464–79.
636 doi:10.1093/femsre/fuw006

637 32. Beek SL van der, Breton YL, Ferenbach AT, Chapman RN, Aalten DMF van, Navratilova I, et al. GacA is
638 essential for Group A *Streptococcus* and defines a new class of monomeric dTDP-4-dehydrorhamnose
639 reductases (RmlD). Mol Microbiol. 2015;98: 946–962. doi:10.1111/mmi.13169

640 33. Ma Y, Pan F, McNeil M. Formation of dTDP-Rhamnose Is Essential for Growth of Mycobacteria. J Bacteriol.
641 2002;184: 3392–3395. doi:10.1128/JB.184.12.3392-3395.2002

642 34. Beek SL van der, Zorzoli A, Çanak E, Chapman RN, Lucas K, Meyer BH, et al. Streptococcal dTDP-L-rhamnose
643 biosynthesis enzymes: functional characterization and lead compound identification. Mol Microbiol.
644 2019;111: 951–964. doi:10.1111/mmi.14197

645 35. Quivey RG, Grayhack EJ, Faustoferri RC, Hubbard CJ, Baldeck JD, Wolf AS, et al. Functional profiling in
646 *Streptococcus mutans*: construction and examination of a genomic collection of gene deletion mutants.
647 Mol Oral Microbiol. 2015;30: 474–495. doi:10.1111/omi.12107

648 36. Kovacs CJ, Faustoferri RC, Quivey RG. RgpF Is Required for Maintenance of Stress Tolerance and Virulence in
649 *Streptococcus mutans*. J Bacteriol. 2017;199. doi:10.1128/JB.00497-17

650 37. De A, Liao S, Bitoun JP, Roth R, Beatty WL, Wu H, et al. Deficiency of RgpG Causes Major Defects in Cell
651 Division and Biofilm Formation, and Deficiency of LytR-CpsA-Psr Family Proteins Leads to Accumulation of
652 Cell Wall Antigens in Culture Medium by *Streptococcus mutans*. Appl Environ Microbiol. 2017;83.
653 doi:10.1128/AEM.00928-17

654 38. Boyle EA, Andreasson JOL, Chircus LM, Sternberg SH, Wu MJ, Guegler CK, et al. High-throughput biochemical
655 profiling reveals sequence determinants of dCas9 off-target binding and unbinding. Proc Natl Acad Sci.
656 2017;114: 5461–5466. doi:10.1073/pnas.1700557114

657 39. Anderson EM, Haupt A, Schiel JA, Chou E, Machado HB, Strezoska Ž, et al. Systematic analysis of CRISPR–
658 Cas9 mismatch tolerance reveals low levels of off-target activity. J Biotechnol. 2015;211: 56–65.
659 doi:10.1016/j.jbiotec.2015.06.427

660 40. Klein M, Eslami-Mossallam B, Arroyo DG, Depken M. Hybridization Kinetics Explains CRISPR-Cas Off-
661 Targeting Rules. Cell Rep. 2018;22: 1413–1423. doi:10.1016/j.celrep.2018.01.045

662 41. Chatterjee P, Jakimo N, Jacobson JM. Minimal PAM specificity of a highly similar SpCas9 ortholog. Sci Adv.
663 2018;4: eaau0766. doi:10.1126/sciadv.aau0766

664 42. Jakimo N, Chatterjee P, Nip L, Jacobson JM. A Cas9 with Complete PAM Recognition for Adenine
665 Dinucleotides. bioRxiv. 2018; 429654. doi:10.1101/429654

666 43. Edraki A, Mir A, Ibraheim R, Gainetdinov I, Yoon Y, Song C-Q, et al. A Compact, High-Accuracy Cas9 with a
667 Dinucleotide PAM for In Vivo Genome Editing. Mol Cell. 2019;73: 714-726.e4.
668 doi:10.1016/j.molcel.2018.12.003

669 44. Bailey J, Cass J, Gasper J, Ngo N-D, Wiggins P, Manoil C. Essential gene deletions producing gigantic bacteria.
670 PLOS Genet. 2019;15: e1008195. doi:10.1371/journal.pgen.1008195

671 45. Kawai Y, Mercier R, Mickiewicz K, Serafini A, Carvalho LPS de, Errington J. Crucial role for central carbon
672 metabolism in the bacterial L-form switch and killing by β-lactam antibiotics. Nat Microbiol. 2019; 1–11.
673 doi:10.1038/s41564-019-0497-3

674 46. Nakano K, Nomura R, Nakagawa I, Hamada S, Ooshima T. Demonstration of *Streptococcus mutans* with a
675 Cell Wall Polysaccharide Specific to a New Serotype, k, in the Human Oral Cavity. J Clin Microbiol. 2004;42:
676 198–202. doi:10.1128/JCM.42.1.198-202.2004

677 47. Coykendall AL. Classification and identification of the viridans streptococci. Clin Microbiol Rev. 1989;2: 315–
678 328. doi:10.1128/CMR.2.3.315

679 48. Beaussart A, Péchoux C, Trieu-Cuot P, Hols P, Mistou M-Y, F. Dufrêne Y. Molecular mapping of the cell wall
680 polysaccharides of the human pathogen *Streptococcus agalactiae*. Nanoscale. 2014;6: 14820–14827.
681 doi:10.1039/C4NR05280C

682 49. Caliot É, Dramsi S, Chapot-Chartier M-P, Courtin P, Kulakauskas S, Péchoux C, et al. Role of the Group B
683 antigen of *Streptococcus agalactiae*: a peptidoglycan-anchored polysaccharide involved in cell wall
684 biogenesis. PLoS Pathog. 2012;8: e1002756. doi:10.1371/journal.ppat.1002756

685 50. Terleckyj B, Willett NP, Shockman GD. Growth of several cariogenic strains of oral streptococci in a
686 chemically defined medium. Infect Immun. 1975;11: 649–655.

687 51. Zhang Q, Ye Y. Not all predicted CRISPR–Cas systems are equal: isolated cas genes and classes of CRISPR like
688 elements. BMC Bioinformatics. 2017;18: 92. doi:10.1186/s12859-017-1512-4

689 52. Biswas A, Gagnon JN, Brouns SJJ, Fineran PC, Brown CM. CRISPRTarget. RNA Biol. 2013;10: 817–827.
690 doi:10.4161/rna.24046

691 53. Crooks GE, Hon G, Chandonia J-M, Brenner SE. WebLogo: a sequence logo generator. Genome Res. 2004;14:
692 1188–90. doi:10.1101/gr.849004

693 54. Blin K, Pedersen LE, Weber T, Lee SY. CRISPy-web: An online resource to design sgRNAs for CRISPR
694 applications. Synth Syst Biotechnol. 2016;1: 118–121. doi:10.1016/j.synbio.2016.01.003

695 55. Lorenz R, Bernhart SH, Höner zu Siederdissen C, Tafer H, Flamm C, Stadler PF, et al. ViennaRNA Package 2.0.
696 Algorithms Mol Biol. 2011;6: 26. doi:10.1186/1748-7188-6-26

697 56. Jong IG de, Beilharz K, Kuipers OP, Veening J-W. Live Cell Imaging of *Bacillus subtilis* and *Streptococcus*
698 *pneumoniae* using Automated Time-lapse Microscopy. JoVE J Vis Exp. 2011; e3145. doi:10.3791/3145

699 57. Abranches J, Miller JH, Martinez AR, Simpson-Haidaris PJ, Burne RA, Lemos JA. The collagen-binding protein
700 Cnm is required for Streptococcus mutans adherence to and intracellular invasion of human coronary
701 artery endothelial cells. Infect Immun. 2011;79: 2277–2284. doi:10.1128/IAI.00767-10

702
703

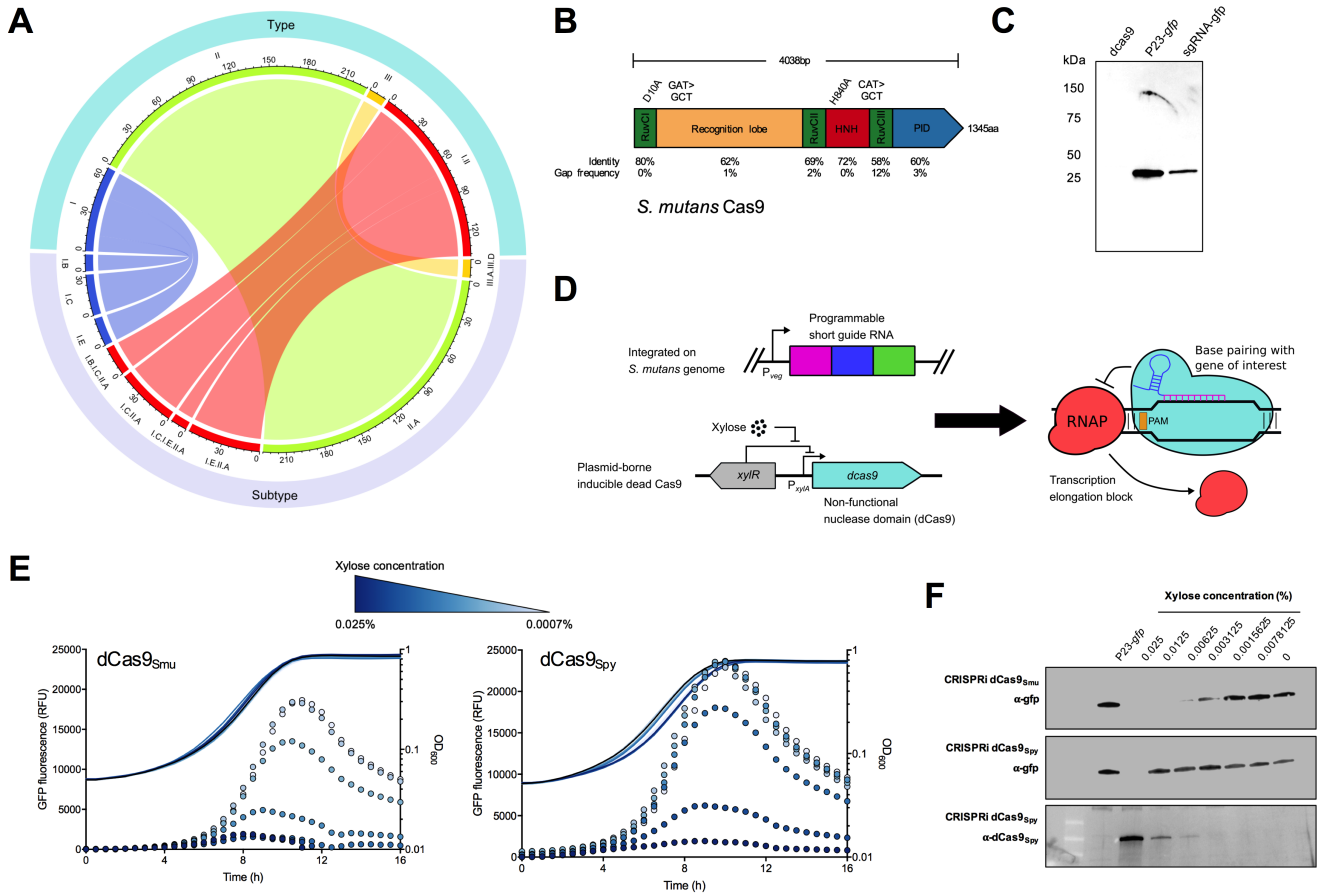

Figure 1. Design of an inducible CRISPRi gene-silencing system for *S. mutans*. (A) Distribution of CRISPR-Cas systems in *S. mutans* by type (top half) and subtype (bottom half). For example, 67 *S. mutans* strains contain Type I systems (blue), and the subtypes of this system are B, C, and E (I-C is the most common). The numbers on the exterior of the plot denote the number of *S. mutans* strains that possess a certain CRISPR-Cas system. (B) Diagram of the Cas9 protein of *S. mutans* UA159 showing domains. The two conserved amino acids required for nuclease activity in the *S. pyogenes* Cas9 protein that were mutated to create the *S. mutans* dCas9 protein are indicated. Each domain was compared with *S. pyogenes* Cas9 for percentage amino acid identity. (C) Gene-silencing activity of endogenous $dCas9_{Smu}$ was assessed by expressing an sgRNA with complementarity to a chromosomally integrated *gfp* gene and comparing GFP protein levels using Western blotting (sgRNA-*gfp*). Also shown is a negative control, d*cas9* without *gfp*, and a positive control strain that constitutively expreses the *gfp* gene from the P23 promoter (see text for details). (D) Overview of the CRISPRi system engineered for *S. mutans*, which consists of two primary elements, a chromosomally located sgRNA and a plasmid-borne inducible dead Cas9. Combined, these two elements can block gene transcription as shown on the right. (E) Comparison of $dCas9_{Smu}$ (left) and $dCas9_{Spy}$ (right) *gfp* gene silencing activity using real-time fluorescence monitoring. Fluorescence readings are shown as dots, and cell density (OD_{600}) readings as lines. As the xylose concentration was decreased, data points change from a dark to a light blue color. (F) Comparison of $dCas9_{Smu}$ (top panel) and $dCas9_{Spy}$ (middle panel) *gfp* gene silencing activity with Western blotting as as a function of xylose concentration. The bottom panel is a Western blot against the xylose-inducible $dCas9_{Spy}$; as this antibody detected $dCas9_{Spy}$, but not $dCas9_{Smu}$.

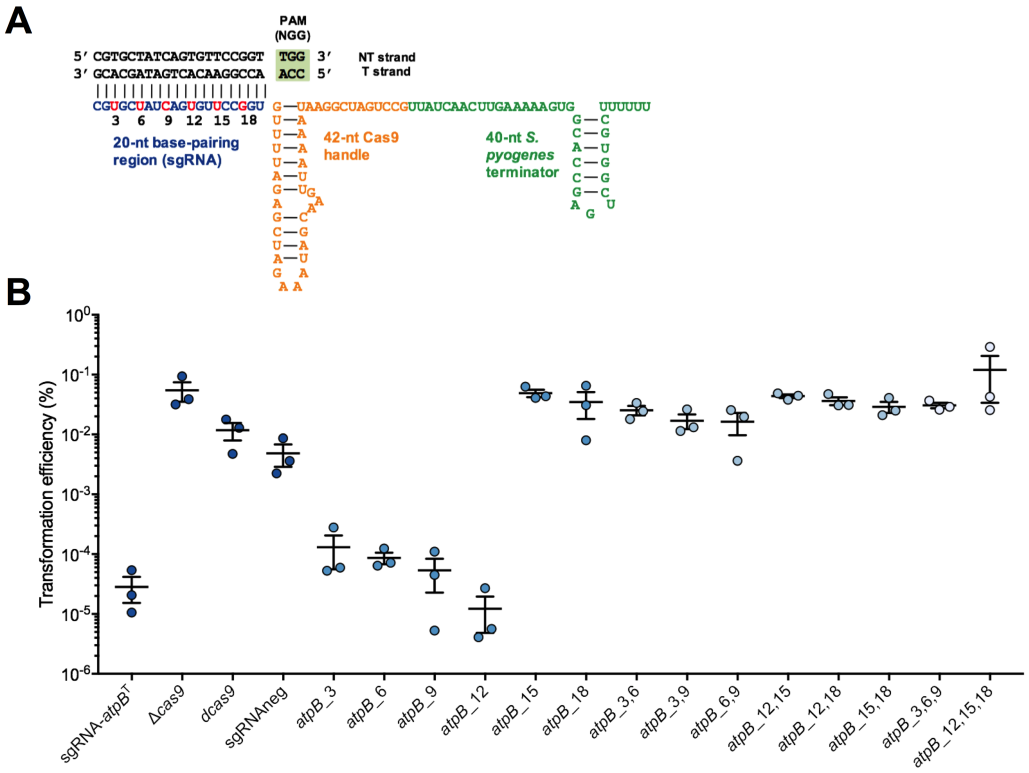

Figure 2. Determining guide RNA specificity of Cas9$_{Smu}$. (A) Diagram of the sgRNA for *atpB* and the mutagenesis strategy. Positions 3, 6, 9, 12, 15 and 18 of the sgRNA were mutated (including in pairs or triplets) as a way of investigating sgRNA specificity (see text for additional details). (B) Plasmid interference assay of wild-type and mutated sgRNA-*atpB* plasmids, with Δ*cas9*, d*cas9* and sgRNAneg serving as controls (for no plasmid interference). If the plasmid interfered with *S. mutans atpB* expression, a lower transformation efficiency would be expected.

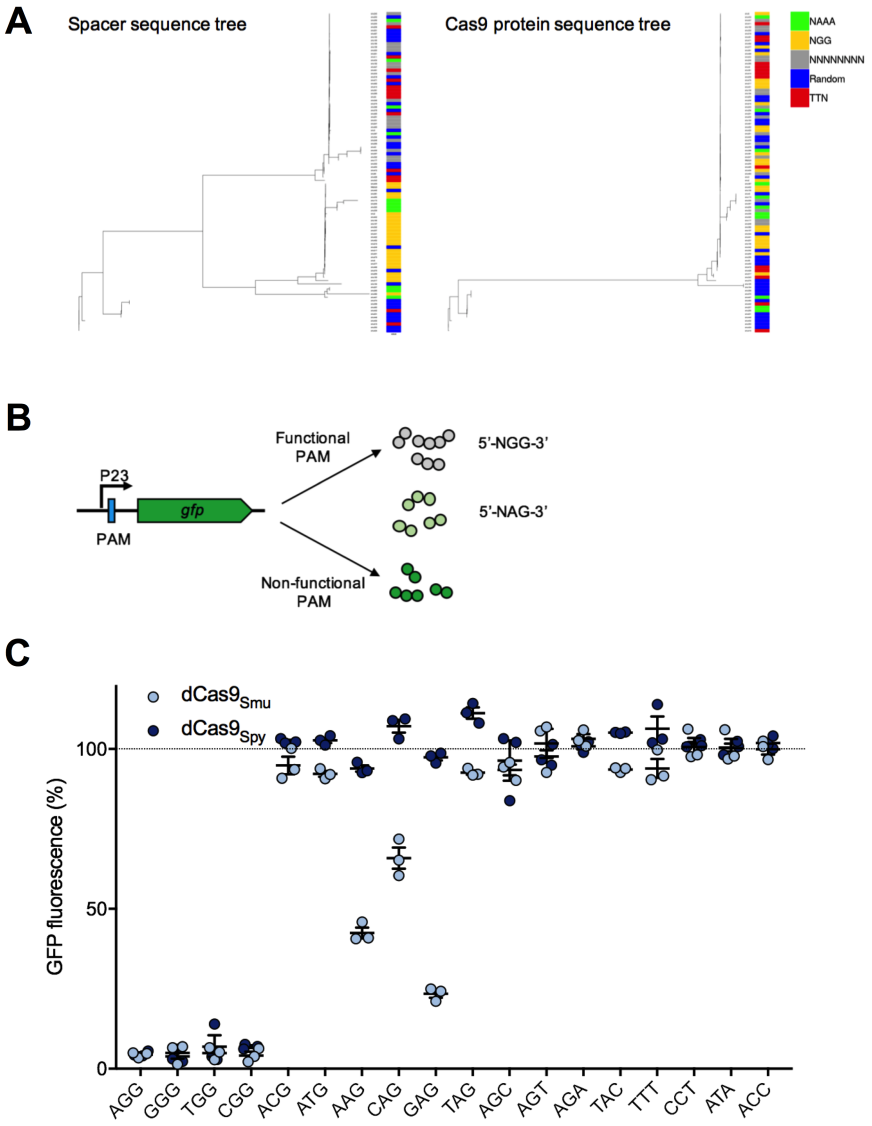

Figure 3. Investigating the proto-spacer adjacent motif (PAM) requirements of $Cas9_{Smu}$. (A) Phylogenetic relatedness of extracted CRISPR-Cas9 spacer sequences (left) and Cas9 protein sequences (right). Consensus PAM sequences were built from spacer sequences and are available in Fig. S3. A key describing the colors chosen for consensus PAM sequences is shown on the far right. (B) To determine the optimal PAM sequence for $dCas9_{Smu}$, different PAM sequences were inserted into between the P23 promoter and *gfp* gene. (C) The functionality of various PAM sequences were compared by measuring CRISPRi repression of GFP fluorescence for both *S. pyogenes* and *S. mutans* Cas9. Repression was calculated as a percentage of maximal fluorescence without exogenous xylose compared to fluorescence with xylose added. Bars show the average and standard deviation, and light blue dots are the individual values, obtained using the $dCas9_{Smu}$ construct, whereas the dark blue dots show data obtained using $dCas9_{Spy}$. Maximal repression was measured with a 5'-NGG-3' PAM, with moderate repression for some 5'-NAG-3' PAMs.

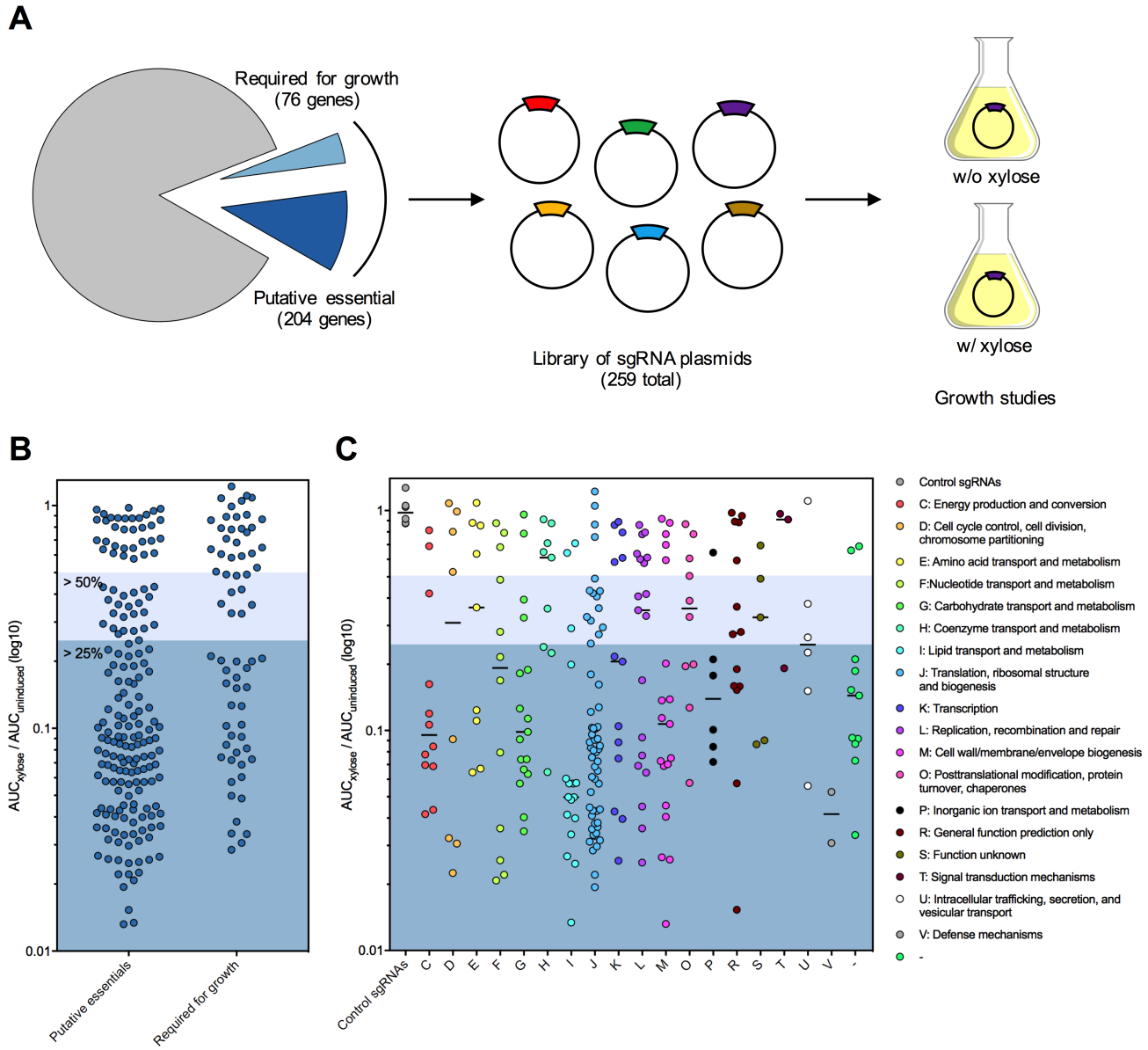

Figure 4. High-throughput growth analysis of a comprehensive library of sgRNAs targeting essential and growth supporting genes. (A) Overview of the CRISPRi growth study that included generating sgRNAs against >250 essential or growth-supporting genes. Growth analysis of CRISPRi strains (B) whether putative essential or required for growth and (C) sorted for physiological functions by Clusters of Orthologous Groups. CRISPRi strains were cultured in the presence or absence of xylose and the area under the curve (AUC) was calculated for each condition. Growth phenotypes were categorized according to the ratio of AUC_{xylose} to $AUC_{uninduced}$ (the lower the number the stronger the growth defect).

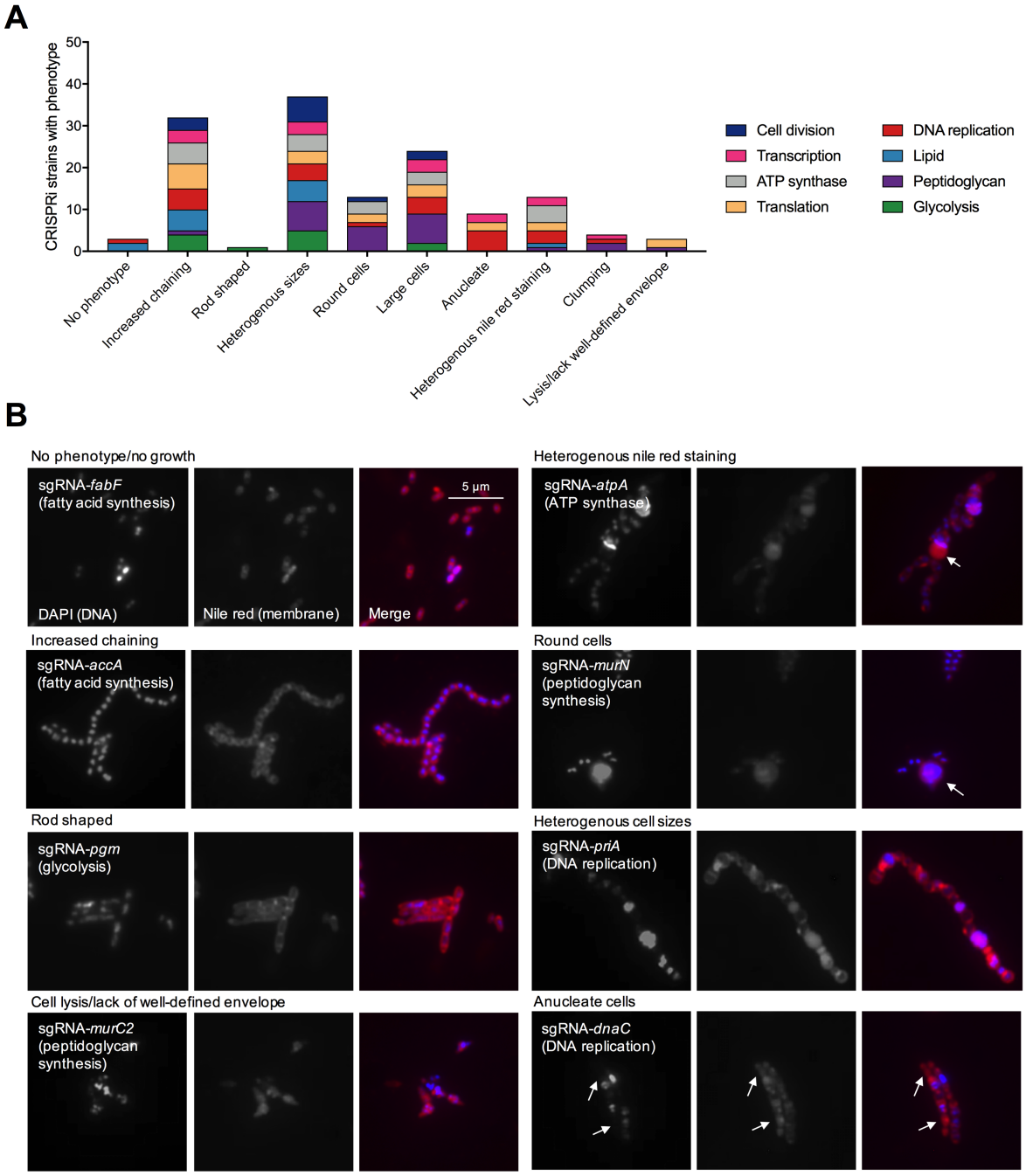

Figure 5. Microscopic analysis of the morphological defects caused by CRISPRi essential gene depletion. (A) CRISPRi strains, by functional pathway, were grouped according to cell morphology phenotypes. Strains with depleted essential genes can have more than one morphological defect (*e.g.* increased cell chaining and heterogeneous sizes). (B) Representative micrographs for several of the cell morphology phenotypes that were observed are shown. Additional microscopy across all the pathways investigated can be found in Figs. S5-S12. For sgRNA-*atpA* the arrow shows an area of increased nile red staining compared to other cells. The large round cells observed when silencing peptidoglycan biosynthesis is depicted with the sgRNA-*murN* micrograph. Arrows indicate potential anucleate cells when targeting the DNA replication-related gene *dnaC*.

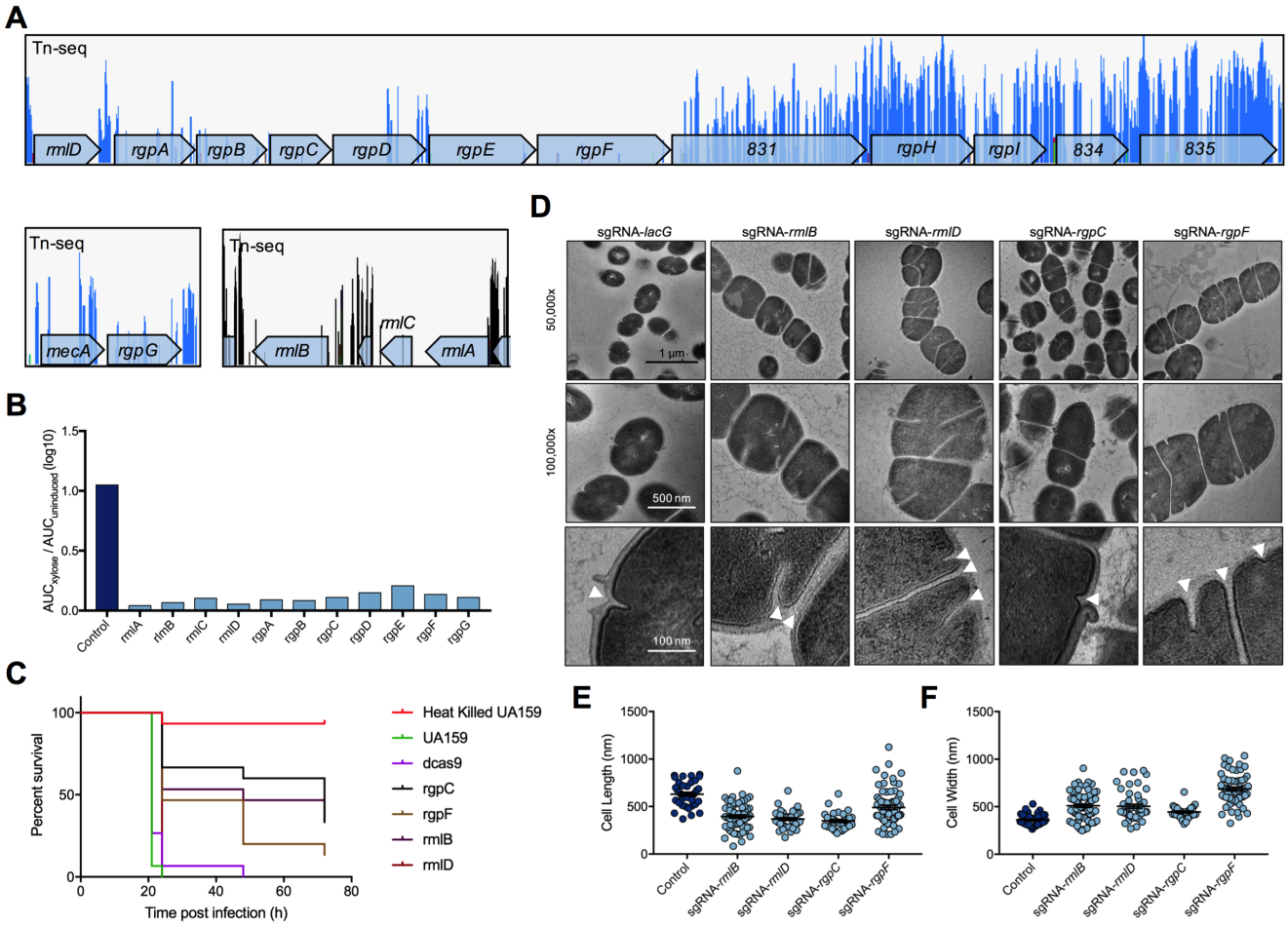

Figure 6. Rhamnose-glucose polysaccharide biosynthesis genes are required for growth, pathogenesis and correct cell division of *S. mutans*. (A) Distribution of Tn-seq reads within genes that function in RGP biosynthesis (*rmlA-rmlC*, *rgpG*, and *rmlD-rgpF*; SMu.831-835 reside in the operon that starts with *rmlD*). Each peak corresponds to a transposon insertion with a lack of peaks within a gene representative of an essential gene (*e.g. rmlA* or *rgpE*). (B) Growth phenotypes of silenced RGP biosynthesis genes compared to a control strain (sgRNA-*lacG*). (C) Pathogenesis phenotypes of silenced RGP biosynthesis genes (*rmlB*, *rmlD*, *rgpC*, and *rgpF*) in a *Galleria mellonella* infection model. Heat killed UA159 served as a negative control, and wild-type UA159 and d*cas9* absent sgRNA as positive controls. (D) Electron micrographs of CRISPRi strains targeting the same genes investigated in the pathogenesis model. Arrowheads point to putative division septa. Fluorescence microscopy images and growth curves for CRISPRi strains for all of the genes involved in this pathway can be found in Fig. S13. Cell length (E) and width (F) measurements from TEM micrographs using ImageJ.

Supplemental Materials and Methods

Strain cloning. Site-directed mutagenesis, using the splice overlap extension method (1), was employed to mutate aspartic acid residue 10 to alanine and histidine residue 840 to alanine within *S. mutans cas9* (SMu.1405c). For each mutation, two PCR products were generated using primers that contained the desired mutations, and primers which annealed 0.6 kbp upstream or downstream of the region of interest. The two PCR products, with 25-bp homology that included the mutation, were subjected to PCR for 1 cycle in the absence of added primers. Next, the outer primers were added and a second PCR of 30 cycles was used to amplify the 1.2 kbp fragment with the desired mutation. Both PCR products (for each mutation) were purified and transformed into competent *S. mutans*. Colonies were selected on the basis of erythromycin resistance using a suicide plasmid carrying an internal fragment of the *lacG* gene. Potential clones containing the desired mutations were screened using PCR and DNA Sanger sequencing. Afterwards, strains that had been selected using the *lacG* plasmid were grown in the presence of lactose, to identify strains that had lost the suicide plasmid and the sensitivity of the strains to erythromycin was used as further confirmation of the plasmid. A Δ*cas9* (SMu.1405c) strain was generated in a similar manner, except here the ATG start codon was mutated to a stop codon (TAG; AT>TA). For marking *S. mutans* with GFP, a fragment of DNA was synthesized that contained the P23 promoter and a synthetic RBS followed by a superfolder *gfp* sequence (2). This fragment was subsequently cloned into the pBGE plasmid that integrates at the *gtfA* locus of *S. mutans* (3). The restriction enzymes *Xba*I and *Bsr*GI were used to clone the DNA fragment into the pBGE plasmid.

Green fluorescent protein PAM comparison assay. PAM sequences were introduced into a P23 promoter driving *gfp* gene expression (pBGE::P23-*gfp*) using the Q5® Site-Directed Mutagenesis Kit. An sgRNA with complementarity adjacent to this PAM was introduced into the pPM::sgRNA plasmid also using the Q5® Site-Directed Mutagenesis Kit. pBGE::P23-*gfp* plasmids (containing PAMs) were introduced into an *S. mutans* strain with a Δ*cas9* mutation and carrying pPM::sgRNA-P23 and P_{xyl}-d$cas9_{Smu}$. GFP fluorescence and microbial growth were measured with a Synergy HT, as detailed in the Materials and Methods section.

Western blotting. Bacterial strains were grown in FMC-maltose (with or without xylose) at 37°C to an OD_{600} of 0.5. Cells were harvested by centrifugation at 3,500 × *g* for 10 min, spent medium was discarded, and cell pellets were stored overnight at −20°C. On the following day, the pellets were resuspended in 100 µl of lysis buffer (60 mM Tris, pH 6.8, 2% sodium dodecyl sulfate [SDS]) and transferred to a screw-cap microcentrifuge tube that contained 100 µl 0.1-mm ice-cold glass beads. Samples were homogenized in a bead beater for 30 s three times with 5-min intervals on ice. The samples were then centrifuged at 8,000 × *g* for 10 min at 4°C. The supernates, which contained the *S. mutans* proteins, were carefully removed and placed into a fresh 1.5-ml microcentrifuge tube. The protein concentration was determined using a bicinchoninic acid (BCA) assay following the supplier's protocol (Pierce), with purified bovine serum albumin used as the standard. Ten µg of each lysate was diluted in 4X SDS loading buffer and the mixture was boiled for 10 min. Proteins were separated by SDS-polyacrylamide gel electrophoresis (PAGE) and then transferred to a polyvinylidene difluoride (PVDF) membrane using a Trans-Blot Turbo transfer system (Bio-Rad). Green fluorescent protein was detected using a polyclonal anti-GFP antibody (1:5,000 dilution; Millipore Sigma) and a goat-anti-rabbit immunoglobulin G (IgG) antibody (1:5,000 dilution; SeraCare Life Sciences, USA). $dCas9_{Spy}$ was detected using a mouse monoclonal anti-CRISPR-Cas9 antibody (1:5,000 dilution; abcam #ab191468) and goat-anti-mouse IgG antibody (1:5,000 dilution; SeraCare Life Sciences, USA). Western blot signals were detected using a SuperSignalWest Pico chemiluminescent substrate kit (Thermo Fisher Scientific) and visualized with a FluorChem 8900 imaging system (Alpha Innotech, USA).

Essential and growth-supporting genes of *S. mutans* UA159

839 Essential genes in *S. mutans* UA159 were identified with Tn-seq performed as described before (4, 5),
840 with slight modifications to growth conditions. Transposon mutants were selected on BHI agar, whereas
841 previous libraries were initially selected on blood agar. After libraries were created and stored in frozen
842 aliquots, they were grown in BHI or FMC for 7-10 generations; previous libraries were passaged for ~30
843 generations. The results of these experiments were used to determine which genes to target with
844 CRISPRi in parallel with previous Tn-seq in *S. mutans* UA159. In addition, for poorly annotated
845 essential or growth-supporting genes we ran the protein sequence through BLASTP.

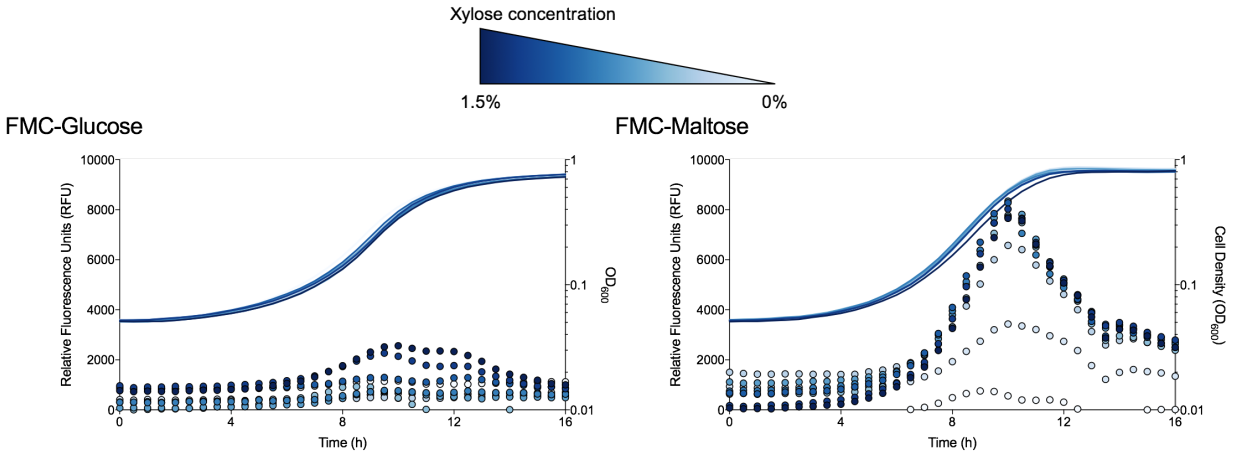

Figure S1. Determining the optimal conditions for xylose induced gene expression in *S. mutans*. The graphs show (glucose left, maltose right) that P_{xyl}-*gfp* expression was higher in FMC-maltose than FMC-glucose for comparable amounts of xylose. Fluorescence readings are shown as dots, and cell density readings as lines. As the xylose concentration is diluted data points change from a dark to a light blue color.

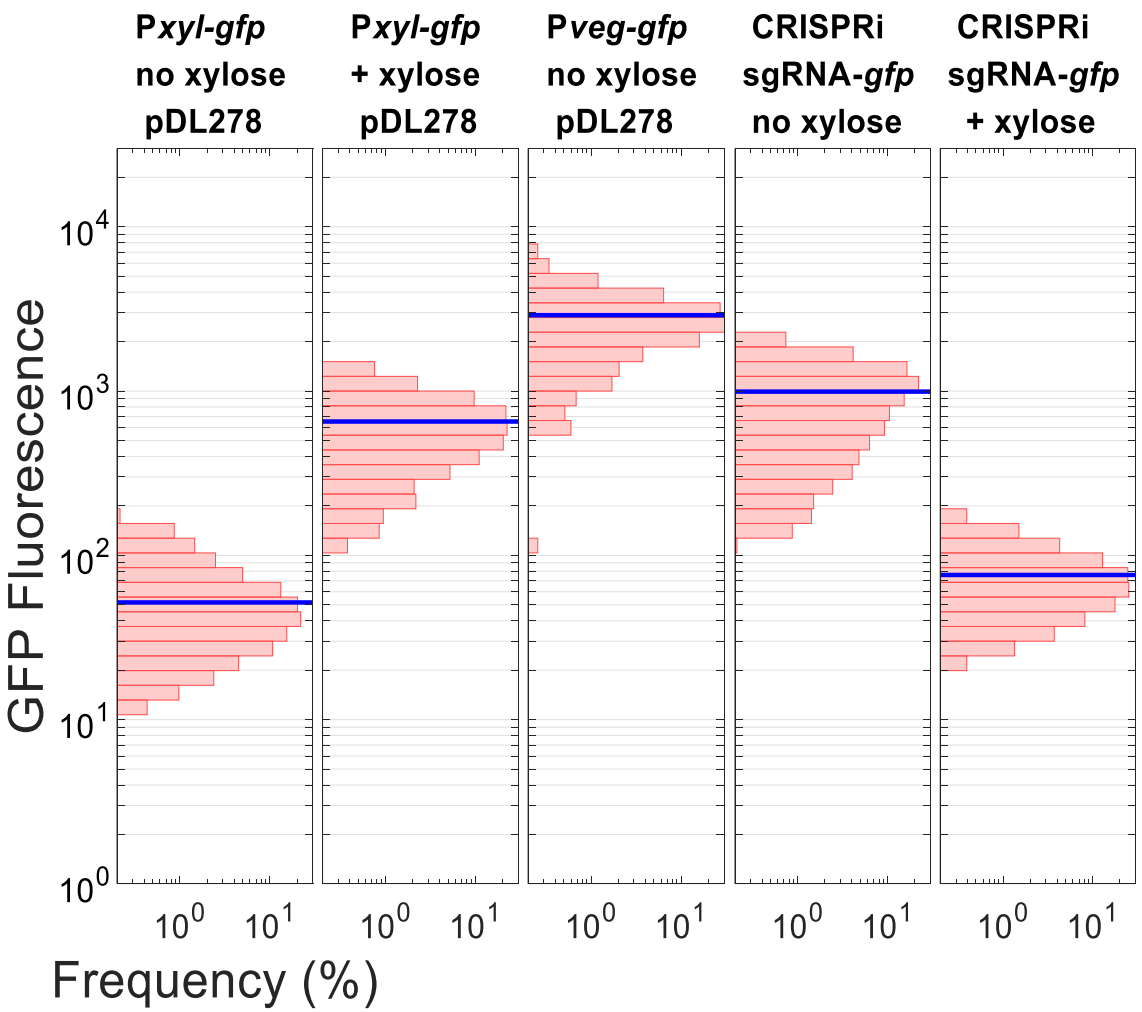

852
853 **Figure S2. Single-cell analysis of P_{xyl}-*gfp* expression and CRISPRi knockdown.** Addition of xylose
854 to FMC-maltose induced *gfp* expression in virtually all imaged cells (first versus second panel) although
855 *gfp* expression was not as high as observed with a constitutive P_{veg} promoter (third panel). In a
856 CRISPRi strain containing a chromosomally integrated *gfp* reporter all cells were GFP positive without
857 xylose addition (fourth panel). Virtually no cells expressed *gfp* when xylose was added to the CRISPRi
858 strain as median GFP fluorescence was barely above background (fifth panel).

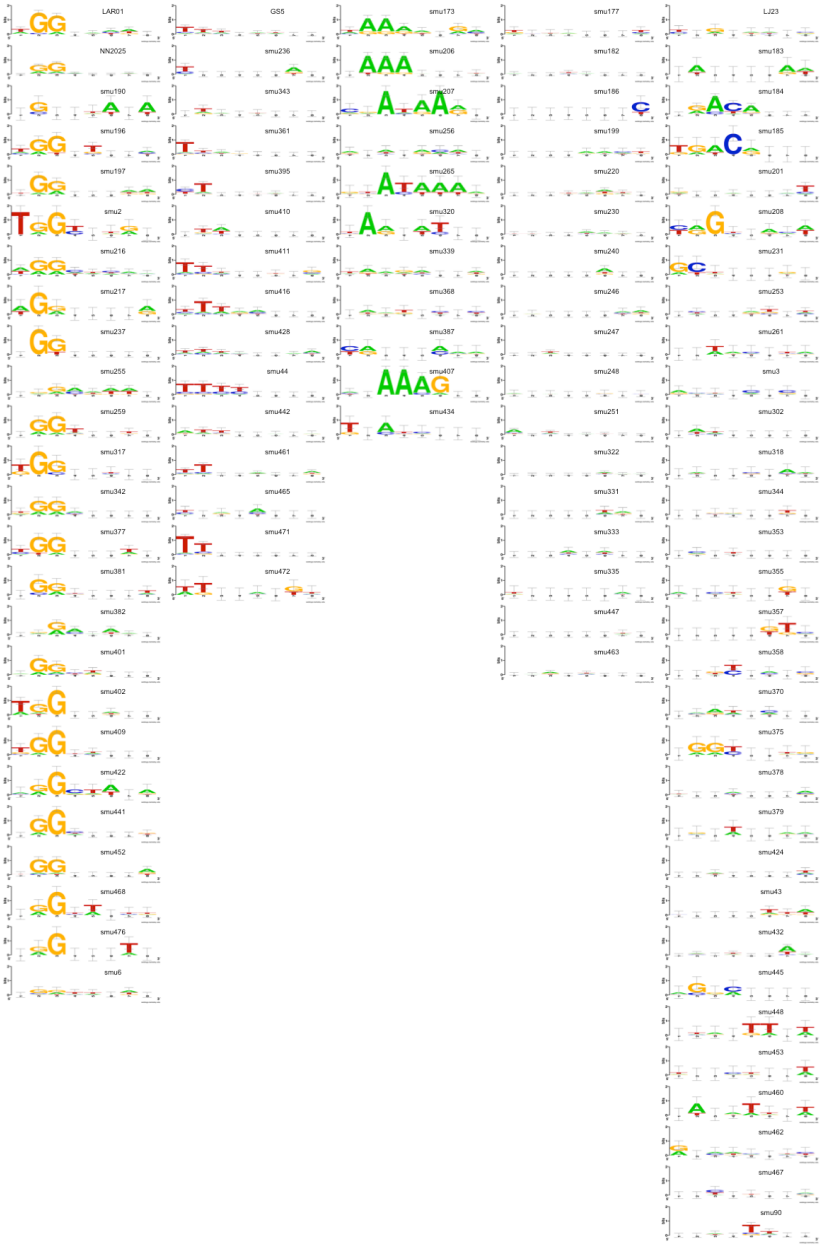

Figure S3. Cas9 PAM predictions for *Streptococcus mutans* strains. Spacer sequences found within Type II CRISPR cassettes of *S. mutans* strains were aligned to the genome of the *Streptococcus* phage M102AD. After alignment protospacer adjacent motifs (PAMs) were extracted and consensus PAMs were generated with WebLogo. Consensus PAMs broadly fit into five groups, 5'-NGG-3', T-rich, A-rich, no distinct PAM and a fifth group of PAMs that didn't fit into the first four groups.

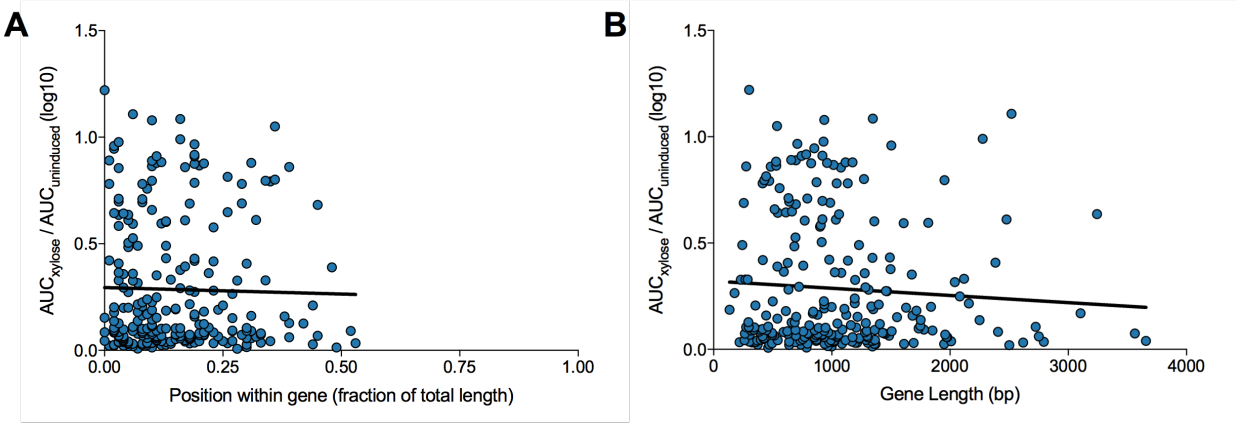

Figure S4. Investigating the impact of sgRNA position within gene and overall gene length on CRISPRi growth defects. (A) Overall, there was no discernable impact on CRISPRi mediated growth defects according to the placement of the sgRNA within the gene. (B) Gene length did not impact CRISPRi-mediated growth defects across all measured strains (*e.g.* larger genes showing stronger growth defects versus smaller genes).

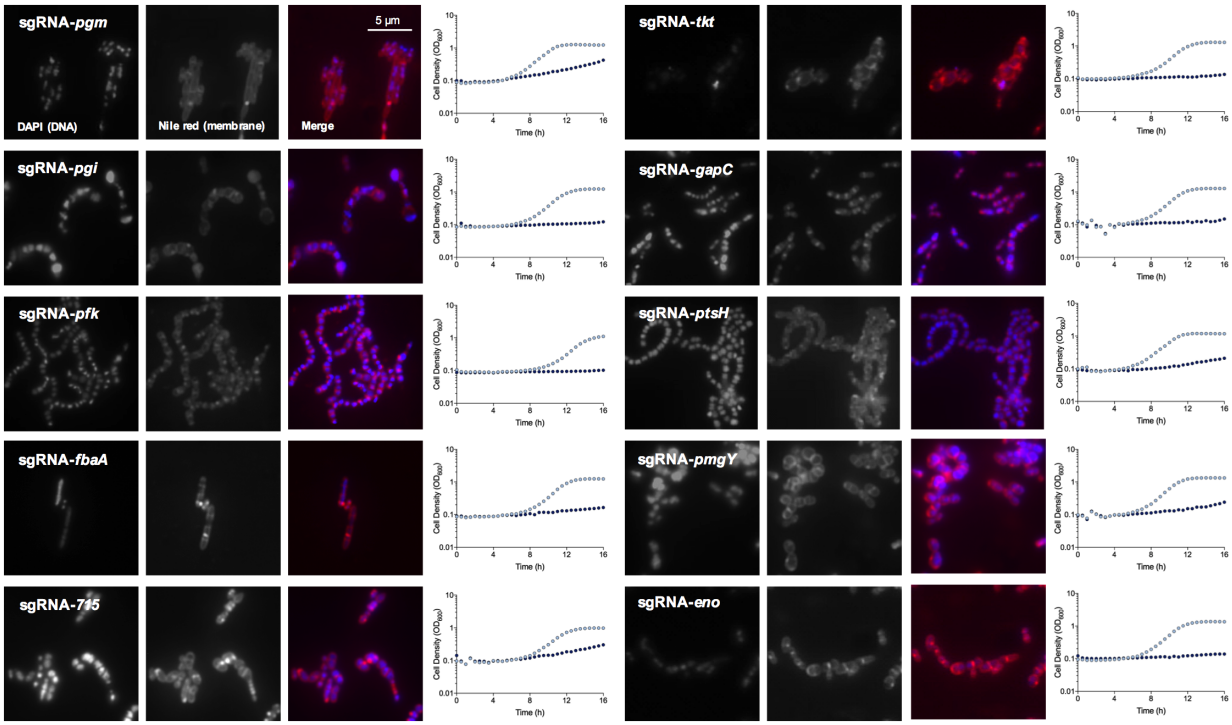

Figure S5. Growth phenotypes and microscopy of CRISPRi strains with silenced genes related to carbohydrate metabolism. For growth assays, light blue dots indicate the no xylose condition and dark blue dots represent the addition of 0.1% xylose. Cells were stained with DAPI (DNA stain) and nile red (membrane stain) and imaged with a x100 oil objective. For each strain a representative microscopic image is shown.

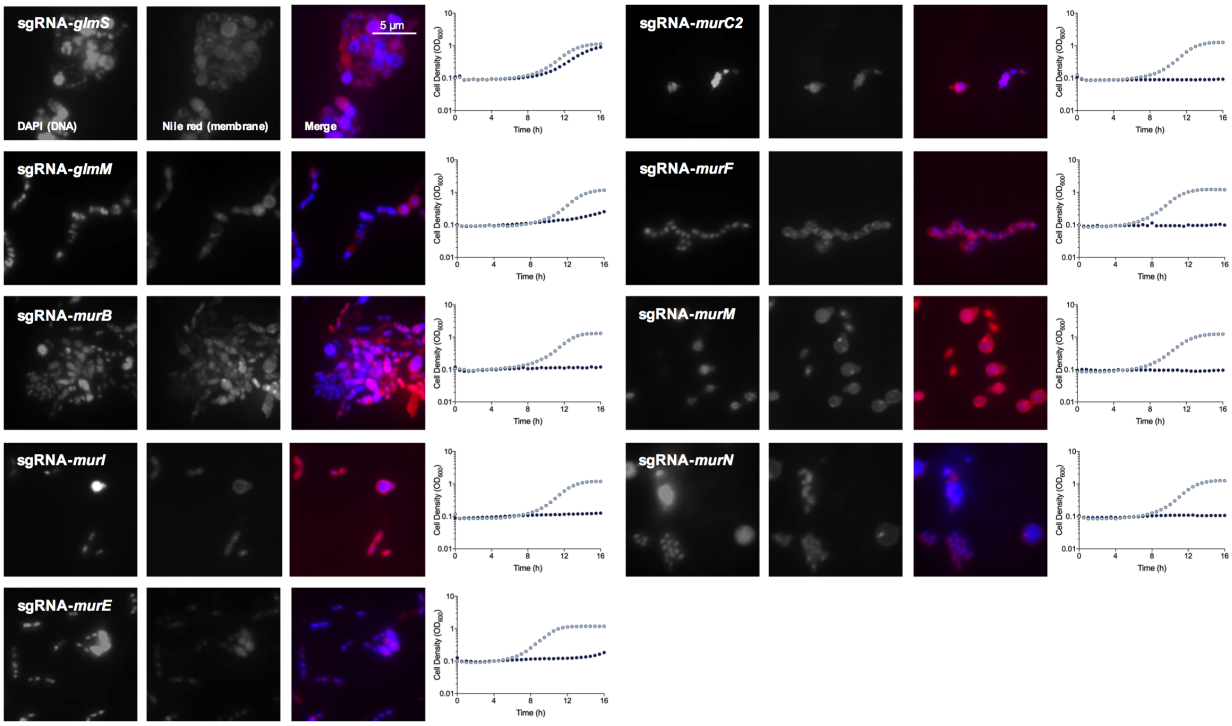

877
878 **Figure S6. Growth phenotypes and microscopy of CRISPRi strains with silenced genes related**
879 **to peptidoglycan biosynthesis.** For growth assays, light blue dots indicate the no xylose condition
880 and dark blue dots represent the addition of 0.1% xylose. Cells were stained with DAPI (DNA stain) and
881 nile red (membrane stain) and imaged with a x100 oil objective. For each strain a representative
882 microscopic image is shown.

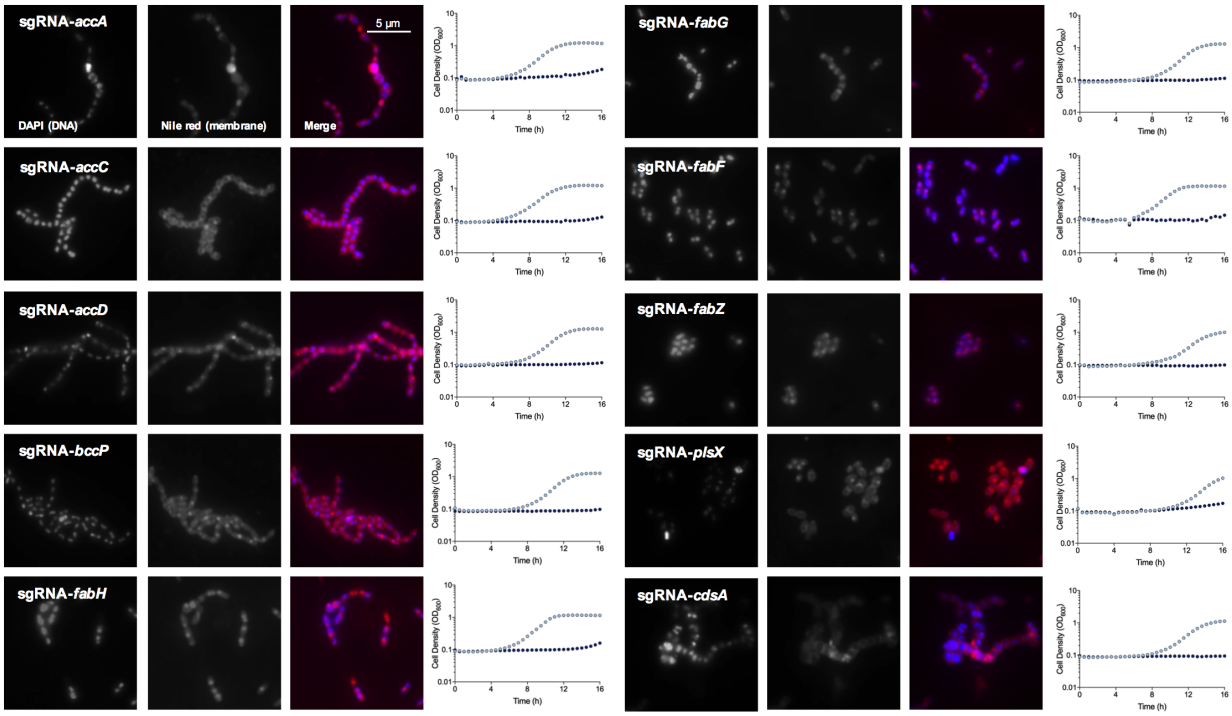

Figure S7. Growth phenotypes and microscopy of CRISPRi strains with silenced genes related to lipid metabolism. For growth assays, light blue dots indicate the no xylose condition and dark blue dots represent the addition of 0.1% xylose. Cells were stained with DAPI (DNA stain) and nile red (membrane stain) and imaged with a x100 oil objective. For each strain a representative microscopic image is shown.

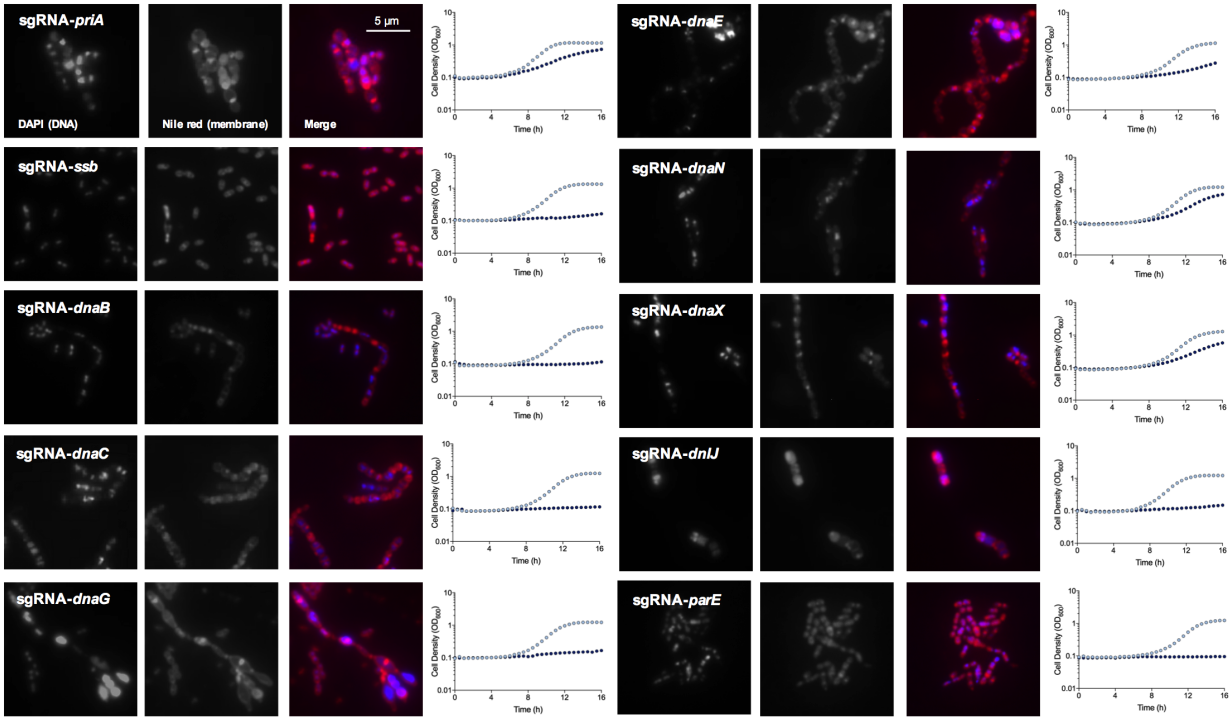

Figure S8. Growth phenotypes and microscopy of CRISPRi strains with silenced genes related to DNA replication. For growth assays, light blue dots indicate the no xylose condition and dark blue dots represent the addition of 0.1% xylose. Cells were stained with DAPI (DNA stain) and nile red (membrane stain) and imaged with a x100 oil objective. For each strain a representative microscopic image is shown.

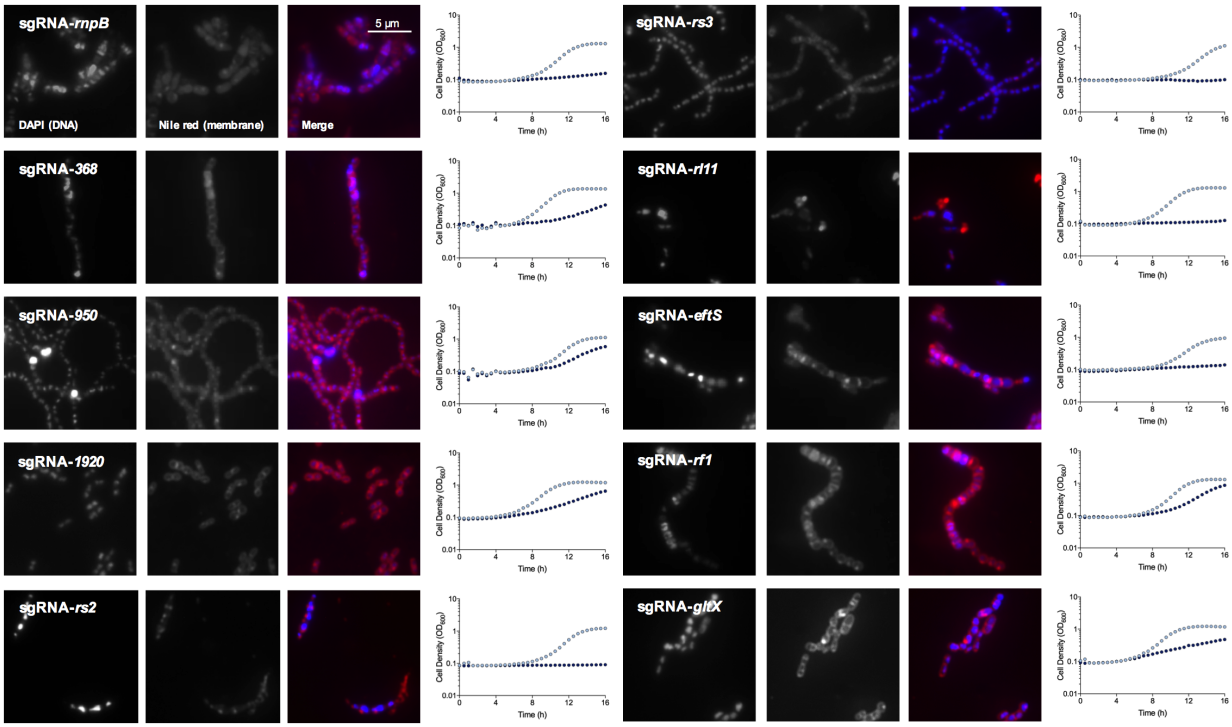

Figure S9. Growth phenotypes and microscopy of CRISPRi strains with silenced genes related to translation and ribosome biogenesis. For growth assays, light blue dots indicate the no xylose condition and dark blue dots represent the addition of 0.1% xylose. Cells were stained with DAPI (DNA stain) and nile red (membrane stain) and imaged with a x100 oil objective. For each strain a representative microscopic image is shown.

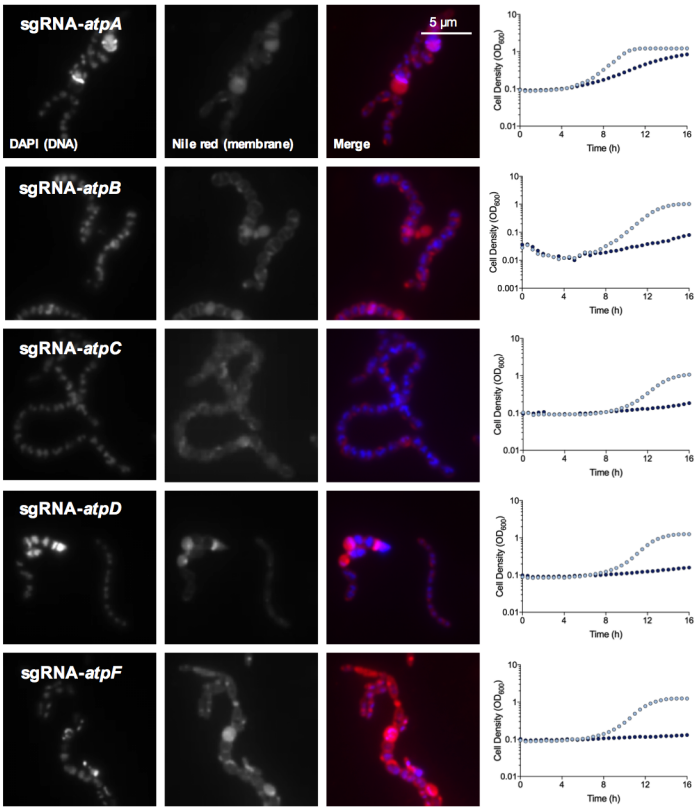

Figure S10. Growth phenotypes and microscopy of CRISPRi strains with silenced genes related to ATP synthase activity. For growth assays, light blue dots indicate the no xylose condition and dark blue dots represent the addition of 0.1% xylose. Cells were stained with DAPI (DNA stain) and nile red (membrane stain) and imaged with a x100 oil objective. For each strain a representative microscopic image is shown.

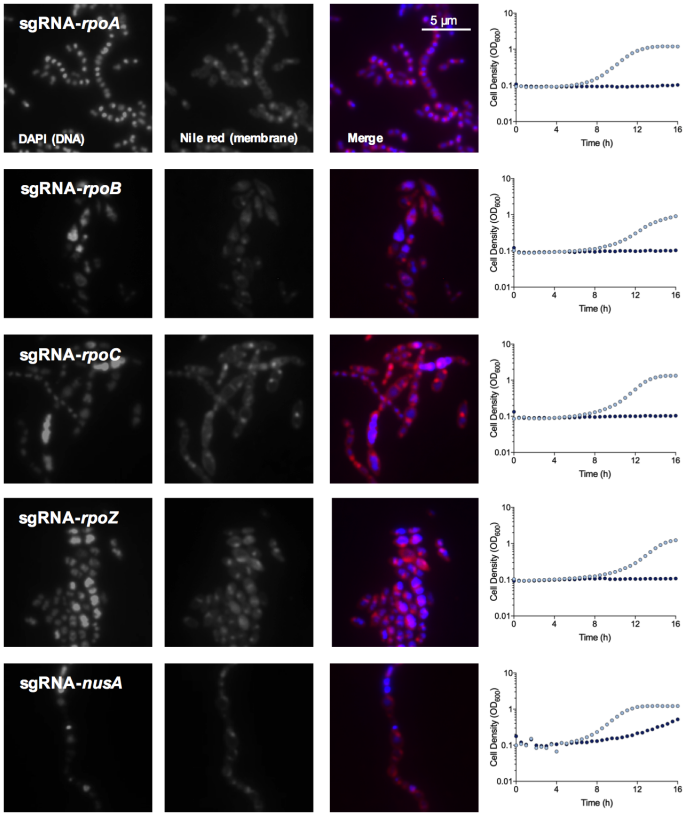

Figure S11. Growth phenotypes and microscopy of CRISPRi strains with silenced genes related to transcription. For growth assays, light blue dots indicate the no xylose condition and dark blue dots represent the addition of 0.1% xylose. Cells were stained with DAPI (DNA stain) and nile red (membrane stain) and imaged with a x100 oil objective. For each strain a representative microscopic image is shown.

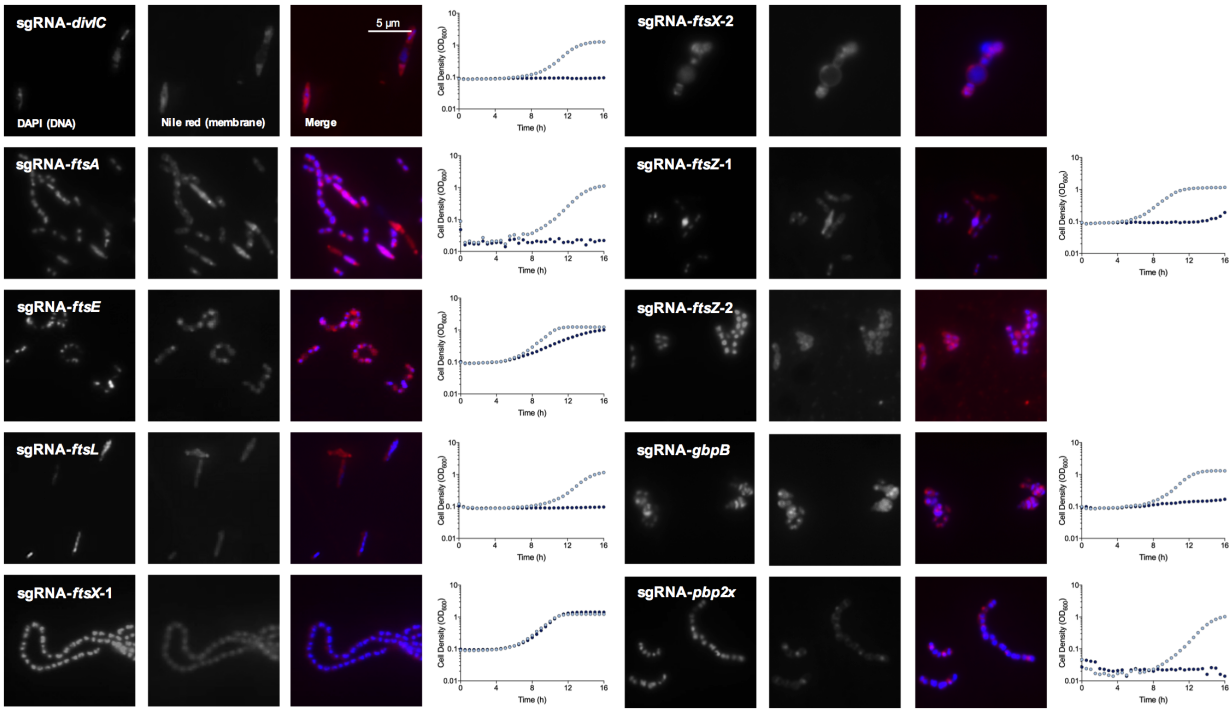

Figure S12. Growth phenotypes and microscopy of CRISPRi strains with silenced genes related to cell division. For growth assays, light blue dots indicate the no xylose condition and dark blue dots represent the addition of 0.1% xylose. Cells were stained with DAPI (DNA stain) and nile red (membrane stain) and imaged with a x100 oil objective. For each strain a representative microscopic image is shown.

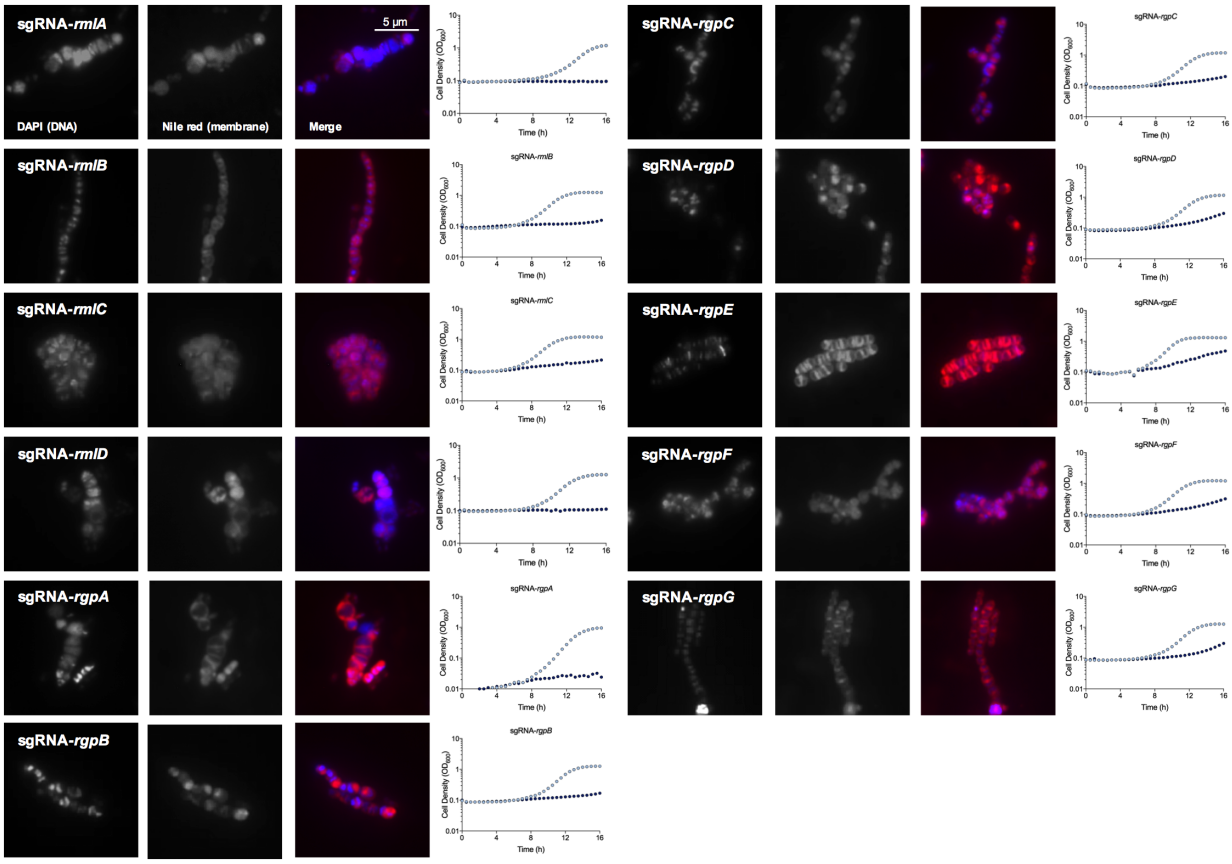

Figure S13. Growth phenotypes and microscopy of CRISPRi strains with silenced genes related to rhamnose-glucose polysaccharide biosynthesis and transport. For growth assays, light blue dots indicate the no xylose condition and dark blue dots represent the addition of 0.1% xylose. Cells were stained with DAPI (DNA stain) and nile red (membrane stain) and imaged with a x100 oil objective. For each strain a representative microscopic image is shown.

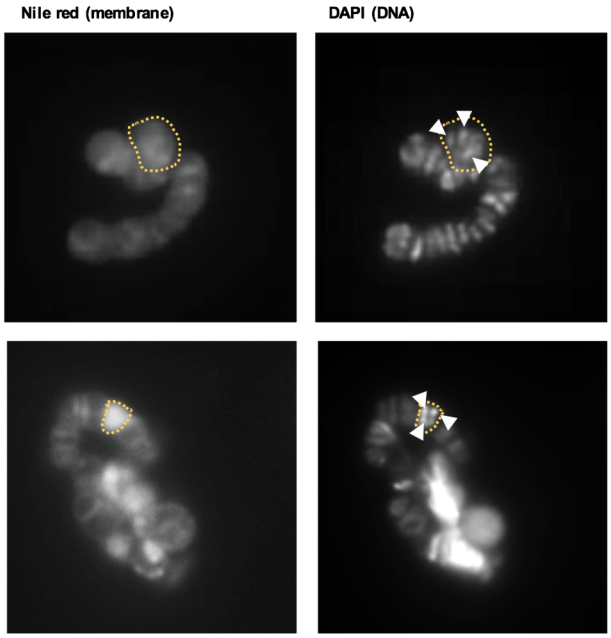

Figure S14. Multiple nucleoids per cell for RGP biosynthesis knockdowns. Cell borders are shown with dotted orange lines. Inside outlined cells multiple nucleoids are visible as punctate bright dots, also highlighted with white arrowheads.

930 **Supplemental Text References**

931 1. Ho SN, Hunt HD, Horton RM, Pullen JK, Pease LR. 1989. Site-directed mutagenesis by overlap
932 extension using the polymerase chain reaction. Gene 77:51–59.
933 2. Shields RC, Kaspar JR, Lee K, Underhill S a. M, Burne RA. 2019. Fluorescence tools adapted for
934 real-time monitoring of the behaviors of Streptococcus species. Appl Environ Microbiol.
935 3. Zeng L, Burne RA. 2009. Transcriptional Regulation of the Cellobiose Operon of Streptococcus
936 mutans. J Bacteriol 191:2153–2162.
937 4. Shields RC, Zeng L, Culp DJ, Burne RA. 2018. Genomewide Identification of Essential Genes and
938 Fitness Determinants of *Streptococcus mutans* UA159. mSphere 3:e00031-18.
939 5. Shields RC, O'Brien G, Maricic N, Kesterson A, Grace M, Hagen SJ, Burne RA. 2018. Genome-
940 wide screens reveal new gene products that influence genetic competence in *Streptococcus*
941 *mutans*. Journal of Bacteriology 200:16 e00508-17.
942
943